The University of Manchester

Modelling of Crevice Corrosion Kinetics in Stainless Steel

A thesis submitted to the University of Manchester for the degree of Master of Philosophy in the Faculty of Science and Engineering

2022

Mayamin Razali

School of Natural Sciences

Department of Materials

Table of Contents

List of Figures

CHAPTER 4

List of Tables

Abstract

Understanding corrosion kinetics is of high importance because it has a significant adverse effect on the economics and sustainability of various industries. My research work aimed to investigate the crevice corrosion kinetics in iron nuts and bolts. 2-Dimensional simulation models of iron nuts and bolts were simulated in Comsol Multiphysics software. This research provides insight into the crevice corrosion mechanism and factors that are affecting it. Corrosion kinetics for iron in 10 M and 0.01M NaCl solution, is different, especially inside the crevice. For instance, the peak pH value at the bottom of the crevice in 10M and 0.01M NaCl solution are 10.4 and 11.5, respectively. In addition to that, the lowest potential value at the bottom of the crevice in 10M and 0.01M NaCl solutions were found to be -365 mV and -790mV, respectively. In this work, the crevice corrosion mechanism is closely followed by the passive dissolution theory. One of the key findings in my research is that position in the geometry affects the oxygen concentration, and subsequently affects the pH and the corrosion thermodynamic characteristics. In 1M NaCl solution, in 20 μm crevice width, at the bottom of crevice, the oxygen concentration depleted after 8 min, where pH was estimated to be 8.5, and the metal entered the active region as shown in pourbaix diagram (fig. 4-9). Moreover, the relationship between crevice width-depth and oxygen concentration was investigated. The simulation revealed that the oxygen concentration inside the crevice depletes completely. On the contrary, the outer crevice did not deplete. The simulations showed that smaller crevice width and larger crevice depth have higher oxygen depletion rates. At the bottom of the crevice in geometry 1, oxygen depletes completely in 21 min for 50 μm and less than 2 minutes for 5 μm crevice width. Moreover, it took less than 0.5 min for a 5 μm crevice width to deplete its oxygen completely in the geometry that has twice the depth. Oxygen diffusion into the crevice was found to be limited, especially for the smaller and deeper crevice. The results presented in this thesis help the industrial partner Grundfos, to simulate the effect of salt solution and geometry in an occluded region.

Declaration

No portion of the work referred to in the thesis has been submitted in support of an application for another degree or qualification of this or any other university or other institute of learning.

Copyright Statement

i. The author of this thesis (including any appendices and/or schedules to this thesis) owns certain copyright or related rights in it (the "Copyright") and s/he has given The University of Manchester certain rights to use such Copyright, including for administrative purposes.

ii. Copies of this thesis, either in full or in extracts and whether in hard or electronic copy, may be made only in accordance with the Copyright, Designs and Patents Act 1988 (as amended) and regulations issued under it or, where appropriate, in accordance with licensing agreements which the University has from time to time. This page must form part of any such copies made.

iii. The ownership of certain Copyright, patents, designs, trademarks and other intellectual property (the "Intellectual Property") and any reproductions of copyright works in the thesis, for example graphs and tables ("Reproductions"), which may be described in this thesis, may not be owned by the author and may be owned by third parties. Such Intellectual Property and Reproductions cannot and must not be made available for use without the prior written permission of the owner(s) of the relevant Intellectual Property and/or Reproductions.

iv. Further information on the conditions under which disclosure, publication and commercialisation of this thesis, the Copyright and any Intellectual Property and/or Reproductions described in it may take place is available in the University IP Policy (see http://documents.manchester.ac.uk/DocuInfo.aspx?DocID=24420), in any relevant Thesis restriction declarations deposited in the University Library, The University Library's regulations (see http://www.library.manchester.ac.uk/about/regulations/) and in The University's policy on Presentation of Theses

Acknowledgments

For Papa,
Mohd Razali bin Matharsha.

Firstly, I would like to express my gratitude to Allah for helping me get through some challenging phases in my life, especially during this past two years, where I experienced so much in a short period; I welcomed my beautiful baby girl, I adapted to covid-19 pandemic lockdown and I believe that my beloved father is in a good place.

Thank you to my daughter, father, mother, husband, and sisters for your love and continuous support. Thank you, Dr. Nicholas Stevens, for your support since 2017 and for sharing your know-how. Thank you Prof. Dirk Engelberg for your advice since 2017 and your continuous support, especially during this uncertain time. Thank you to Dr. Anthony Cook and all personnel from Grundfos that were involved in this project, for the support and useful discussions are appreciated. Thank you CDT M4DE and Grundfos for the funding.

1.0 Introduction

1.1 Corrosion

Corrosion as defined by Fontana[1] is “a destruction or deterioration of a material because of reaction with its environment”. Corrosion can be defined as a chemical or electrochemical reaction between a material and its environment that deteriorates the material and its properties.

Corrosion has affected many areas ranging from marine and aerospace to buildings and roads. According to NACE international report[2], the total cost of corrosion on a global scale in 2013 was USD 2.5 trillion. Corrosion is affecting the industrial sector the most with a cost of USD 1.45 trillion, followed by the service sector with a cost of USD 9 billion. The implementation of corrosion prevention and control is estimated to decrease corrosion-associated costs by 15–35%, however, these saving do not include human safety and environmental issues.

Corrosion can be classified into eight forms[1] which are uniform, galvanic, pitting, crevice, intergranular, leaching, erosion, and stress corrosion. Uniform corrosion is the most common corrosion and corrosion occurred uniformly over the exposed area. Galvanic corrosion is also known as corrosion of dissimilar metals, and it is driven by the potential difference with lower potential metal corroding preferentially. Pitting corrosion is a form of localised corrosion, and it forms cavities on metals, and the pits are usually covered by an oxide layer. Crevice corrosion is a form of localised corrosion, where the localised attack occurs in occluded regions or shielded areas.

Intergranular corrosion is localised attack at and next to the grain boundaries of an alloy where its elements disintegrate and lose their mechanical property. Leaching, which is also known as selective leaching, involves the removal of one element within the alloy such as dezincification. Erosion corrosion involves mechanical movement; particle suspension or liquid impingement, between the fluid and metal surface. Stress corrosion cracking is cracking caused by applied stress and corrosive media.

Crevice corrosion and pitting corrosion are forms of localised corrosion. Localised corrosion is an intensive attack at a higher rate on localised areas on the metal surface, while the rest of the surface is corroding at a much lower rate.

1.2 Crevice Corrosion

Crevice corrosion is a localised corrosion in occluded regions or adjacent to gaps, with either a metal–metal or metal–non-metal interface. Several authors see the similarity of crevice corrosion with pitting corrosion. Corrosion within the crevice can be divided into the initiation phase and propagation phase, where the rate of metal dissolution is the major factor.

One of the common parameters to rank alloy based on its susceptibility to crevice corrosion is based on the Critical Crevice Temperature (CCT). CCT is a baseline or minimum temperature, where crevice corrosion occurs at least 0.025 mm deep beneath the washer.[3] Table 1-1 indicates the CCT for different types of alloys in 6% ferric chloride solution based on ASTM G48.

Metallic materials tend to corrode in the atmospheric and aqueous environment due to their nature and to lower their free energy in the system. Metallic corrosion is an electrochemical reaction consisting of anodic metal oxidation and cathodic oxidant reduction. In principle, metals discharge electrons, which form metal ions as an anodic reaction. Meanwhile, hydrogen atoms or oxidants accept electrons forming hydrogen molecules or hydroxides, respectively as a cathodic reaction. The reduction of hydrogen atoms is predominant in acidic conditions, meanwhile reduction of oxidants is predominant in neutral and basic conditions.

$2\mathrm{Fe} \rightarrow 2\mathrm{Fe}_{\mathrm{aq}}^{2+} + 4\mathrm{e}^-$	Anodic- metal oxidation
$2\mathrm{H}^+ + 2\mathrm{e}^- \rightarrow \mathrm{H}_2$	Cathodic- hydrogen reduction (acidic)
$\mathrm{O}_2 + 2\mathrm{H}_2\mathrm{O} + 4\mathrm{e}^- \rightarrow 4\mathrm{OH}^-$	Cathodic- oxidant reduction (neutral/basic)

Anodic and cathodic reactions occur in a coupled manner at different places on the metal surface. This is due to the heterogeneous nature of the metal surface, where various crystal

faces, grain boundaries, impurity, and defects (edges, screw dislocation, kink, step, and point defects) occur.

Table 1- 1: Critical Crevice Temperature (CCT) for alloys in ferric chloride-based standard solutions.[4]

UNS	EN	CCT (°C)
S31603	1.4436	<0
S32101	1.4162	<0
S32304	1.4362	<0
S31803/32205	1.4462	20
S32750	1.4410	35
S32760	1.4501	35

1.2.1 Thermodynamics of corrosion

The tendency of metallic materials to corrode depends on the spontaneity of a reaction. Gibbs free energy determines the spontaneity of a reaction by quantifying changes in enthalpy and entropy and as indicated in equation (1). ΔG^{o} indicates Gibbs free energy in standard condition, R indicates gas constant of $8.314\ J.mol^{-1}K^{-1}$, T indicates temperature, and K indicates constant.

$$\Delta G = \Delta G^{o} + RT\ \ln K \qquad (1)$$

Meanwhile, free energy for the electrochemical process when all reactants and products are in standard states is given by equation (2), where n is the number of electrons transferred, F is a Faraday constant of $96485\ C$, and E^{o} is the standard electrode potential.

$$\Delta G = -nFE^{o} \qquad (2)$$

The relationship of both equations of free energies in equations (1) and (2), yield the Nernst equation, which relates cell reactions to standard cell potential, equation (3)

$$E = E^{o} - \frac{R\,T}{n\,F}\ln K \qquad (3)$$

Nernst equation is the basis construction of the pourbaix diagram, which predicts the tendency of metallic corrosion, and is illustrated in Fig. 1-1. Corrosion occurs in the region where ferrous ions Fe^{2+}, ferric ions Fe^{3+}, and hydrated iron oxide ions, $Fe(OH)_3^-$ are stable. In the region where, iron oxides, Fe_2O_3 and Fe_3O_4, are stable and form a passive film on the metal surface, no corrosion occurs. In addition, no corrosion occurs in the region where metal iron, Fe is stable.

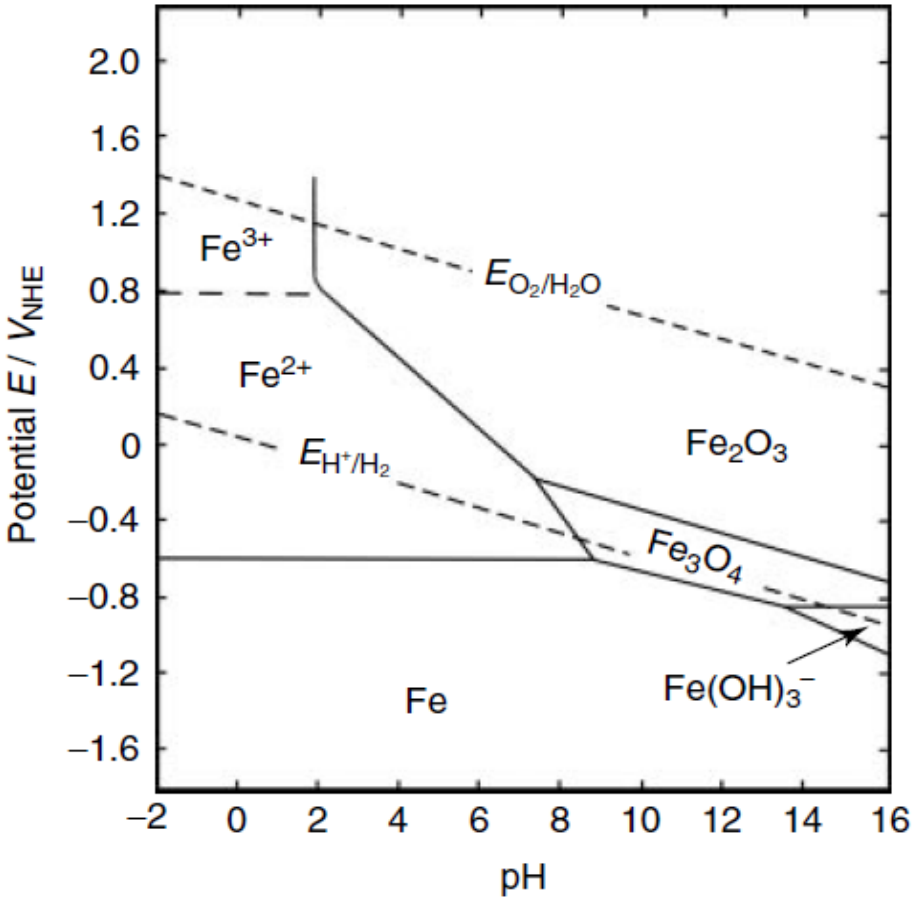

Fig.1- 1: Pourbaix diagram of iron, potential as a function of pH.[5]

1.2.2 Kinetics of corrosion

Thermodynamic approaches do not give information on the rate of corrosion. Therefore, the kinetics of corrosion gives information on how fast or slow corrosion takes place. The corrosion rate can be determined by electrochemical technique as direct current (DC) and alternating current (AC) polarization method. The rates of reaction occurring during the initiation, and propagation of crevice corrosion is different. Total electrochemical polarisation, which is also known as overpotential, is the summation of activation, concentration, and ohmic polarisation as expressed in equation (4).

$$\text{Overpotential}, \eta = \eta_{\text{activation}} + \eta_{\text{concentration}} + \eta_{\text{resistance}} \quad (4)$$

Activation polarization or energy is the energy required to transfer electrons to and from the electrode into the electrolyte. Activation polarisation is a rate-limiting step, where the electrochemical process is limited by the metal-electrolyte interface. Activation polarisation for anodic and cathodic reactions can be evaluated individually based on the Butler-Volmer equation (5). Butler-Volmer equation assumed that electrochemical processes (anodic and cathodic reactions) occur on the same electrode. This equation provides the rate of electrochemical reaction by relating the dependency of potential with current on an electrode.

$$i = i_a - i_c = i_o \left[\exp\left(\frac{\propto_a F \eta}{R T}\right) - \exp\left(\frac{-\propto_c F \eta}{R T}\right) \right] \quad (5)$$

Where i is the net overall current density, i_a is the anodic current density, i_c is the cathodic current density and i_o is the exchange current density (A.cm^{-2}). $\propto_a$ is the anodic charge transfer and $\propto_c$ is the cathodic charge transfer (value in between 0 to 1). F is the faraday constant (96485 C.mol^{-1}). η is the overpotential (V). R is the gas constant (J.mol^{-1}.K^{-1}). T is the temperature (K).

Ohmic polarisation is a polarisation caused by IR or a potential drop in the electrolyte. The electrochemical process of an anodic or cathodic reaction is obstructed by a potential drop in

an electrolyte. The potential drop could also occur across surface films due to the existence of oxides or salts. Concentration polarisation is controlled by concentration adjacent to the metal interface, either concentration of reactant or product. At a faster rate of an electrochemical process than the rate of diffusing species, the concentration of species at metal surface changes compare to its bulk concentration. Current become limited by the rate of chemical species that diffuse on the metal surface. This limiting rate is expressed in equation (6).

$$I_L = \frac{D_i n F C_{B,i}}{x} \qquad (6)$$

I_L is a limiting current, D_i is the coefficient of diffusion for species I ($cm^2.s^{-1}$), n is the number of electrons in the electrochemical process, F is the Faraday constant (96485 $C.mol^{-1}$), $C_{B,i}$ is the bulk concentration of species i ($mol.cm^{-3}$), x is the thickness layer of diffusion (cm).

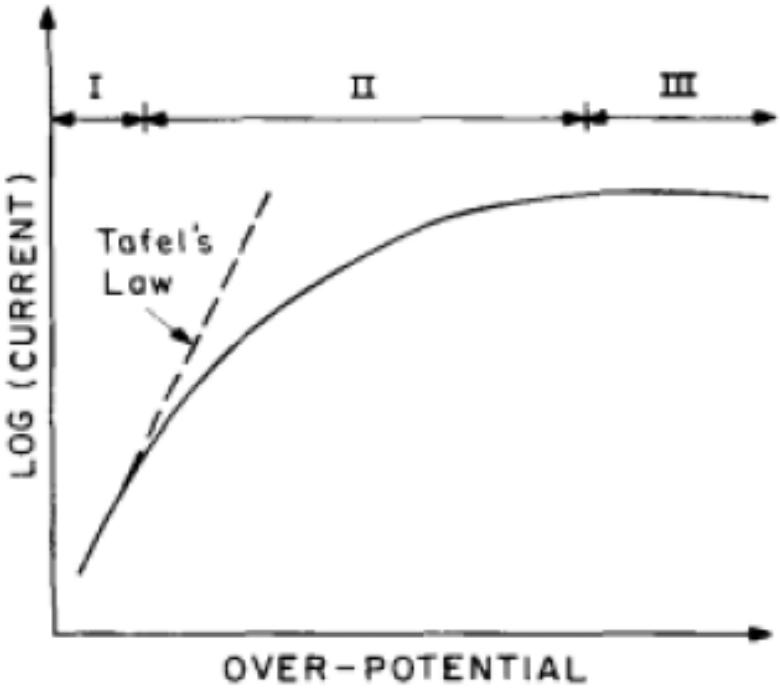

Fig.1- 2: Activation polarisation in region (I); Ohmic polarisation in region (II); Concentration polarisation in region (III).[6]

1.2.3 Mass transport

Chemical species in the electrolyte and at the interface of metal-electrolyte are changing constantly due to the electrochemical and chemical processes. Chemical species are constantly consumed and produced which leads to the continuous movement of species in the electrolyte and on the metal surface. This movement of species is known as 'mass transport'. Mass transport occurs due to diffusion, migration, convection, or a combination of all. Diffusion is a movement of chemical species through a concentration gradient. Migration is the movement of charged particles in an electric field. Convection occurs due to the difference in forces within the electrolyte which includes mechanical intervention such as stirring. The total flux (J_i) of chemical species (i) during mass transport is the summation of diffusion, migration, and convection and is expressed in equation (7).

$$J_i = -D_i \frac{\partial C_i}{\partial x} - z_i \frac{D_i F}{R_g T} C_i \frac{\partial \emptyset}{\partial x} + C_i u \qquad (7)$$

$D_i \frac{\partial C_i}{\partial x}$ is the term for diffusion, $z_i \frac{D_i F}{R_g T} C_i \frac{\partial \emptyset}{\partial x}$ is the term for migration and $C_i u$ is the term for convection.

Diffusion occurs when chemical species move from a high concentration region to a lower concentration region in the electrolyte. The diffusion process is based on Fick's first and second law. Fick's first law describes the diffusion of species as a function of concentration over time. Fick's first law expressed in equation (8) is applicable in a steady state system.

$$J_{D,i}(x) = -D_{x,i} \frac{\partial C_i}{\partial x} \qquad (8)$$

Where $J_{D,i}(x)$ (mol.cm^{-2}.s^{-1}) is the diffusion flux for chemical species, i at a distance x (cm) along concentration gradient. $D_{x,i}$ (cm^2.s^{-1}) is the diffusion coefficient for chemical species, i in x-direction. C_i (mol.cm^{-3}) is the concentration of chemical species, i.

Fick's second law is applicable to determine the change in species concentration at any time in a fixed volume, at any position (x), and expressed in equation (9).

$$\frac{\partial \mathrm{C_i}}{\partial \mathrm{t}} = -\mathrm{D_{x,i}} \frac{\partial^2 \mathrm{C_i}}{\partial \mathrm{x}^2} \tag{9}$$

Migration is the movement of charged particles in an electric field and potential gradient. Migration transportation usually occurs in the bulk solution where the gradient of concentration is low and therefore current is being carried by migration. Flux by migration is expressed in equation (10).

$$\mathrm{J_{M,i}} = -\mathrm{z_i} \frac{\mathrm{D_i F}}{\mathrm{R_g T}} \mathrm{C_i} \frac{\partial \emptyset}{\partial \mathrm{x}} \tag{10}$$

$\mathrm{J_{M,i}}$, is flux due to the migration, $\mathrm{z_i}$ is a charge of ionic species, $\mathrm{D_i}$ is the diffusion coefficient ($\mathrm{cm^2.s^{-1}}$), F is the Faraday constant, $\mathrm{R_g}$ is the gas constant ($\mathrm{J.mol^{-1}.K^{-1}}$), T is a temperature, $\mathrm{C_i}$is the concentration of charged species ($\mathrm{mol.cm^{-3}}$), $\frac{\partial \emptyset}{\partial \mathrm{x}}$ is the potential gradient.

Convection is a movement of chemical species due to forces gradient or intervention mechanical. There are two categories of convection, namely natural and forced convection. Natural convection occurs due to the effect of electrochemical and chemical reactions such as metal dissolution on the electrode. Meanwhile forced convection occurs with external mechanical intervention such as a pump or stirring. Flux by convection is expressed in equation (11).

$$\mathrm{J_{c,i}} = \mathrm{C_i u} \tag{11}$$

$\mathrm{J_{c,i}}$ is a flux due to convection, $\mathrm{C_i}$ is the concentration of dissolved species ($\mathrm{mol.cm^{-3}}$), and u is the velocity of electrolyte ($\mathrm{cm.s^{-1}}$). One of the methods to measure the velocity of electrolytes is via flow meter as fluid flowing from one point to another.

1.2.4 Corrosion Rate

The corrosion rate expressed in equation (12) is based on Faraday's Law. Corrosion rate (CR) is commonly measured in terms of metal thickness that is corroded per year (mm/yr).

$$\mathrm{CR} = \frac{\mathrm{I\,M_w}}{\mathrm{n\,F\,\rho\,A}}\ x\ (3.1536\ x\ 10^{8}) \qquad (12)$$

Where I is the current (A), $\mathrm{M_w}$ is the molecular weight of metal (g.mol^{-1}), n is the number of electrons transferred, F is the Faraday Constant (96485 C.mol^{-1} or A.s.mol^{-1}), ρ is the density (g.cm^{-3}), A is the area of metal or electrode (m^2).

1.3 Research aims and objectives

The aim of this research is to investigate crevice corrosion kinetics in iron nuts and bolts. In order to achieve the aim, several approaches have been taken including:

- To simulate iron nut and bolt geometry that represents crevice. (chapter 4)
- To investigate the influence of solution ionic strength on the pH and potential inside and outside of crevice. (see subchapter 4.1)
- To investigate the influence of positions in geometry on the pH and oxygen concentration within the crevice and outside of the crevice. (see subchapters 4.1 and 4.2)
- To investigate the relationship between the size of crevice width and depth of crevice to the oxygen concentration inside and outside of crevice. (see subchapter 4.2)

2.0 Literature Review

2.1 Mechanism and Theory

In the early 1950s, Evans[7] stated that the primary reason behind intensive corrosion in the crevices was due to lack of oxygen inside the crevice. This statement was also supported by Schaefer[8] in the 1960s, where he stated that initiation location for crevice corrosion is greatly influenced by the area that lacks oxygen (or inhibitor). In addition, Schafer[9] denied the theory of metal ion concentration cell[10] mechanism as a valid explanation for the cause of crevice corrosion. He denied the metal ion concentration cell mechanism because it assumes that; the metal ion concentration at the source is lower and the cell is not self-sustaining due to the absence of cathodic reaction. Meanwhile, Hoar[11] and Uhlig[12,13] studied the mechanism for localised corrosion (pitting) and stated that the breakdown of passive film is due to the adsorption of stronger anions (chloride ions) that displace oxygen on the metal surface.

2.1.1 Passive Dissolution Theory

The mechanism proposed by Fontana and Green[1], and advanced by Oldfield and Sutton[14], consists of four steps; (i) deoxygenation in a crevice solution, (ii) metal hydrolysis and decrease in pH, (iii) breakdown of the passive film and critical crevice solution, and (iv) self-sustaining corrosion.

Initially, both anodic and cathodic reactions occurred on stainless steel that is immersed in a neutral chloride solution containing dissolved oxygen. Metal dissolution and oxygen reduction are anodic and cathodic reactions, respectively, and the overall reaction forms the passive metal oxide film. These reactions occur uniformly, inside and outside of crevice.

Anode: $\mathrm{M} \rightarrow \mathrm{M}^{z+} + \mathrm{z}e^{-}$

Cathode: $\frac{1}{2}\mathrm{O}_2 + \mathrm{H}_2\mathrm{O} + 2e^{-} \rightarrow 2\mathrm{OH}^{-}$

Overall reaction: $2\mathrm{M} + \frac{z}{2}\mathrm{O}_2 + \mathrm{z}\mathrm{H}_2\mathrm{O} \rightarrow 2\mathrm{M}(\mathrm{OH})_z$

Anodic reaction (metal dissolution) is balanced by the cathodic reaction of oxygen reduction. Within the crevice, as more oxygen is reduced, that leads to a reduction in oxygen concentration. Unlike the outer surface where it is relatively easy for oxygen to diffuse on the surface and supply the oxygen for the cathodic process. Inside the crevice, due to the narrow gap a crevice, it is a challenge for oxygen to diffuse into the crevice and this causes oxygen depletion. Oxygen depletion inside the crevice is the indication of the first stage in passive dissolution theory. In the second stage, the anodic reaction continues to occur within the crevice and is maintained by a cathodic reaction outside of the crevice. Thus, to minimise the potential energy and balance the redox reactions, chloride ions diffuse from the bulk solution into the crevice (other anions such as hydroxide ions probably diffuse as well but are less mobile). Metal cations from the anodic reaction react with chloride ions and water, undergoing a hydrolysis reaction, forming metal hydroxides and hydrochloric acid. Precipitation of metal hydroxides removes the hydroxides and leaves the hydrogen ions in the crevice solution, thus increasing the acidity and reducing the pH in the crevice solution.

Hydrolysis reaction: $\mathrm{M^{z+}Cl^{-}} + \mathrm{H_2O} \leftrightarrow \mathrm{MOH^{(z-1)}} + \mathrm{H^{+}Cl^{-}}$

In the third stage, the amount of hydrogen and chloride ions in the solution increases significantly until it reaches its critical level. This critical level is referred to as Critical Crevice Solution (CCS). A high concentration of hydrogen and chloride ions in the solution causes the breakdown of the passive film within the crevice. A passive film formed in the formation of iron oxide (Fe_3O_4) and iron hydroxide (FeOH). CCS is an important parameter during the incubation period and provides information on crevice initiation on pure metal. CCS is based on the diffusion of chloride ions and the formation of hydrogen ions within the crevice, which cause the breakdown of the passive film and initiate crevice corrosion. Typically, CCS has low pH and high chloride concentration. High temperature, higher chloride, and hydrogen ions concentration lead to an increase in critical passivation potential and current density, which will make it harder for an alloy to passivate or remain in a passive steady state. If a critical level of hydrogen ions and chloride concentration is not achieved, the alloy remains in a passive steady-state.

In the fourth stage, corrosion within the crevice propagates rapidly and is self-sustaining with rapid metal dissolution within the crevice, and oxygen reduction outside of the crevice. In neutral sodium chloride solution, pH within crevice can drop to 2.[34]

However, the study by Lott and Alkire[15] contradicts the passive dissolution theory. The authors found that chromium and hydrogen concentration in crevice solution did not increase during the incubation period, in his study on 304L stainless steels in 0.1 NaCl. The authors found an increase in dissolved chromium concentration only after the breakdown of the passive film. The authors postulated that no chromium ions were present and no acidification within the crevice before the breakdown of the passive film, which contradicts the mechanism in passive dissolution theory.

In addition to that, another study by Nash and Kelly[16] also contradicts the passive dissolution theory. The authors characterized the chemical composition of crevice solution on 304L stainless steels using ion chromatography. The authors found that the pH within the crevice does not fall below the de-passivation pH and the crevice solution is not acidic enough to cause a breakdown of the passive film. The authors also stated that the concentration of transition metal within crevice is low and the chemical species that are present during the incubation period is sulphite. De-passivation pH is dependent on the composition of the stainless steels, with typical values of pH 3.25 for stainless steels containing 13% chromium and pH values of 0.25 for stainless steels containing 22% chromium in 30^{o}C NaCl solution (5%). In addition to that, in 80^{o}C salt solution, the de-passivation pH for 13% Chromium is 3.[35]

Findings by Sridhar and Dunn[17] also contradict the passive dissolution theory. The authors found that a decrease in pH and increase in chloride concentration within crevice occurred only after active corrosion occurred. Their findings support Lott and Alkire[15] and Nash and Kelly[16] findings, where changes in chemical composition within crevices are the result of active crevice corrosion and not the cause that initiates crevice corrosion.

Laycock et al.[18] study the initiation of crevice corrosion for 316L stainless steels. The authors found that initiation of crevice corrosion depends more on the potential and not on the time, as proposed by Oldfield and Sutton[14]. In the study by Laycock et al.[18], upon initiation of crevice

corrosion, they find that the concentration of metal ion is 0.1 M which gives a pH of 2.7, which contradicts with experiment by Oldfield and Sutton[14] with a pH of 1.65. The authors also stated that a pH of 2.7 is relatively low to cause the breakdown of a passive film and observed that corrosion initiate at the crevice mouth and not at the centre of the crevice although pH in the centre of the crevice is lower than crevice mouth. In the study of Laycock et al.[18], within the crevice cavity, the presence of chromium in 316L stainless steel facilitates the formation of a chromium oxide layer, hence protecting the crevice cavity from iron oxidation. This chromium oxide layer on top of the iron oxide layer gives extra protection in the high chloride concentration as described in the third stage of passive dissolution theory.

2.1.2 IR Drop Theory

IR drop or also known as the ohmic potential drop is a potential difference when the current (I) passes through resistance (R). Fig. 2-1 compares the cathodic polarisation curve with IR drops represented by a dashed line and without IR drops represent by the dotted line. It can be seen from fig. 2-1 that potential drop due to the resistance in the electrolyte (dash line) is lower compared to potential drop without resistance in the electrolyte (dotted line). This potential drop due to resistance in the electrolyte is known as IR drop. Apart from that, it is shown that the cathodic polarisation curve with IR drop intersects with the anodic polarisation curve, in the active region (and below $\mathrm{E_{crit}}$). Meanwhile, the cathodic polarisation curve without IR drop does not intersect with the anodic polarisation curve.

Kinetic Corrosion Diagram
Potential (E) Vs Current Density (log i)

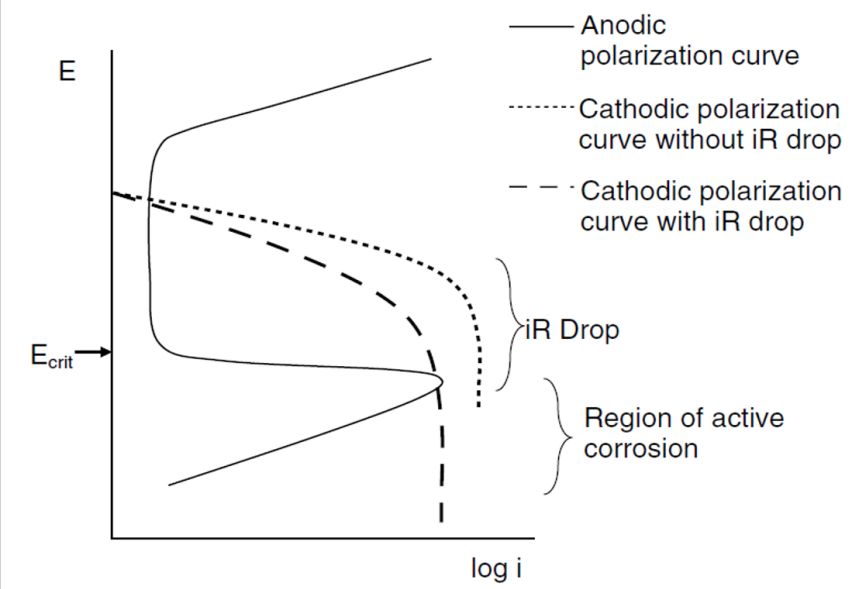

Fig.2- 1: Idealized kinetic corrosion diagram for passive metal. [19]

Pickering and Frankenthal [20] compare the potential difference in crevice mouth and crevice tip for stainless steels and found that the potential in crevice tip is very low (-0.2 V) and potential at crevice mouth is high (+1.4 V), with the potential difference of 1.6 V. The authors postulated that a higher concentration of hydrogen ions in the crevice tip is the primary reason for lower potential in the crevice tip. Besides that, a study by Sridhar and Dunn[17] founds that initially, the potential at crevice mouth and crevice tip is similar and potential difference occurred after initiation of crevice corrosion. Laycock et al.[18] simulated the IR drop mechanism with their study of 316L stainless steel. However, the authors found there is no presence of an active loop in the polarisation curve and thus the authors proposed the use of more aggressive chemistry of crevice solution.

2.1.3 Inclusion Dissolution Theory

Several studies[15–17] have found that chemical composition in crevice solution does not change before to the initiation of corrosion, as suggested by passive dissolution theory and IR drop theory. Hence, another theory has been proposed, which explains how the role of inclusion within the metal affects the initiation of crevice corrosion.

This theory developed and proposed by Alkire and Lott[21,22] is also known as inclusion dissolution theory. They study the role of inclusions during the initiation of crevice corrosion for 304 stainless steels in 0.1 NaCl solution. They stated that crevice geometry, inclusion density, and applied potential are the factors that affect the initiation of crevice corrosion, based on the proposed mechanism. A smaller crevice gap will limit the movement of thiosulfate ions from the crevice and thus increase the chances of the breakdown of a passive film. Higher manganese sulfide inclusion density will increase the production of thiosulfate ions and increase the chances of breakdown and shorter the breakdown time. Application of cathodic protection to crevice will lower the potential, thus lowering the concentration of thiosulfate ions and decreasing the chance of crevice corrosion initiation. In their experiment by Alkire and Lott[21,22], the authors limit only sulfur and thiosulfate presence in the solution and there are no additional species produced in the solution during the oxidation of manganese sulfide to produce thiosulfate. The authors proposed a reaction sequence below, where manganese sulfide (MnS) oxidizes and produces thiosulfate ions ($\mathrm{S_2O_3^{2-}}$), followed by further dissolution of MnS to produce elemental Sulfur,(S). $2\mathrm{MnS} + 3\mathrm{H_2O} \leftrightarrow \mathrm{S_2O_3^{2-}} + 2\mathrm{Mn^{2+}} + 6\mathrm{H^+} + 8\mathrm{e^-}$ and $2\mathrm{H^+} + \mathrm{MnS} \leftrightarrow \mathrm{Mn^{2+}} + \mathrm{S} + \mathrm{H_2}$.

However, a study by Nash and Kelly[16] discussed that only sulphite was found during the induction time and this contradicts with the study by Alkire and Lott[21,22], where they proposed the build-up of thiosulfate ions during the induction period which is before the initiation of crevice corrosion initiation. Apart from that, the study by Laycock et al.[18] shows that the concentration of thiosulfate ions was low and had no significant impact on the pitting potential of 316 L stainless steel in their study. The authors also pointed out that crevice corrosion initiation occurred at a much lower potential than the potential of manganese sulfide dissolution.

2.1.4 Metastable Pitting Theory

Metastable pitting theory is another theory that was developed to explain the initiation mechanism of crevice corrosion from another perspective, rather than changes in chemical composition causing and initiating crevice corrosion, this theory stated it is vice versa. Metastable pitting theory assumed that crevice corrosion is a geometrically stabilised form of

pitting and was developed by Stockert and Bohni[23]. Stockert and Bohni[23] stated that there is an average number of metastable pits that occurred before the initiation of crevice corrosion. Metastable pits occurred both outside and inside of the crevice, and metastable pits that occurred within the crevice can initiate crevice corrosion. Meanwhile, induction time is the time delay before the pit is initiated at a specific site within the crevice.

A metastable pit is protected by a porous pit cover that provides an ohmic drop in the bottom of the pit hence it is in an active state. The pit cover also stabilises the pit and acts as a diffusion barrier to maintain the solution chemistry in the pit. On the open surface, upon rupture of pit cover, the pit precipitates salt film. However, in the crevice, upon rupture of pit cover, narrow crevice geometry is sufficient to act as a barrier and stabilise the pit.

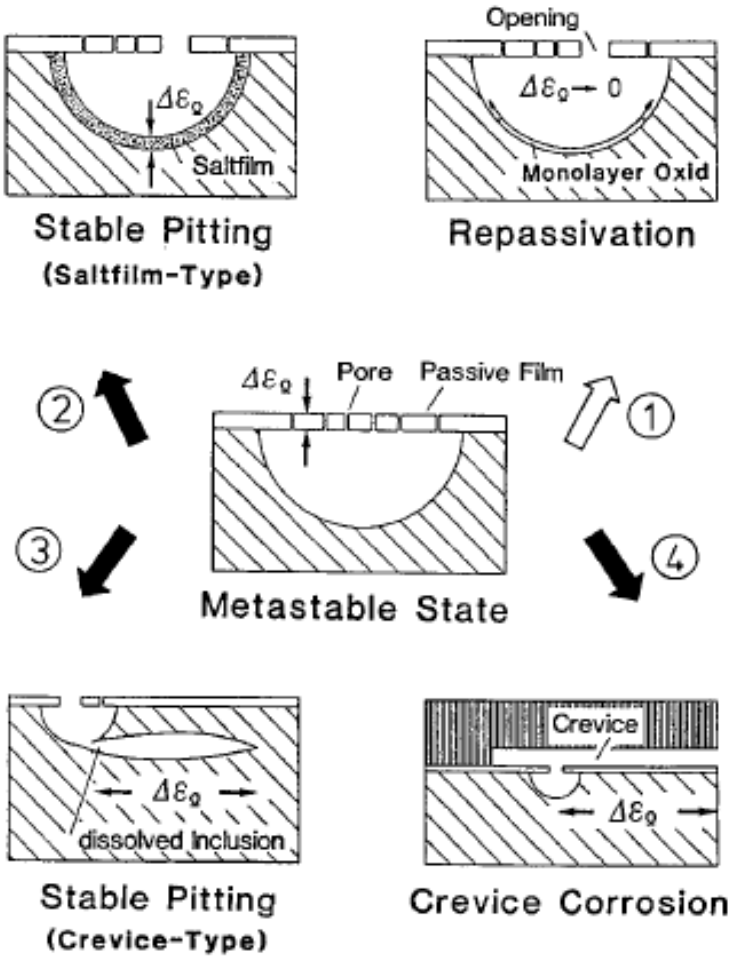

Fig.2- 2: Schematic diagram of four outcomes from a single metastable pit; (1) Repassivation. Pit repassivate due to discontinuity of ohmic potential drop, (2) Stable pitting (salt-film). Growth of pit stabilised when salt film precipitate before rupture of pit cover, (3) Stable pitting (crevice type). Growth of pit influenced by both ohmic drop and charge transfer controlled, (4) Crevice corrosion. Due to crevice geometry, metastable pits initiate crevice corrosion.[23]

Fig. 2-2 shows four different outcomes from a single metastable pit; (1) metastable pit could re-passivate and it re-passivate due to discontinuity of ohmic potential drop, (2) metastable pit could precipitate a salt film within the pit, which if the salt film precipitate before the rupture of pit cover rupture, pit growth will be stabilised, (3) metastable pit could form stable pitting based on crevices and the pit growth influenced by both ohmic drop and charge transfer controlled, (4) metastable pit could initiate crevice corrosion due to its crevice geometry.

Stockert and Bohni[23] developed a transient model to study metastable pit activity and its relation with crevice corrosion. The authors found that metastable pitting is less stable with i Fig. 2-2 shows four different outcome from a single metastable pit; (1) metastable pit could re-passivate and it re-passivates due to discontinuity of ohmic potential drop, (2) metastable pit could precipitate a salt film within pit, which if the salt film precipitate before the rupture of pit cover rupture, pit growth will be stabilised, (3) metastable pit could form stable pitting based on crevices and the pit growth influenced by both ohmic drop and charge transfer controlled, (4) metastable pit could initiate crevice corrosion due to its crevice geometry.

Stockert and Bohni[23] developed transient model to study metastable pit activity and its relation with crevice corrosion. The authors found that metastable pitting is less stable with increasing amount of molybdenum, higher pH value of the solution, lower applied potential value, and lower chloride concentration. In regards to crevice corrosion, the authors pointed out that, within susceptible crevice area (A_w), single metastable pitting activity is the source for initiation of crevice corrosion, which later the crevice corrosion propagates. An increasing amount of molybdenum, higher pH value of the solution, lower applied potential value, and lower chloride concentration. In regards to crevice corrosion, the authors pointed out that, within susceptible crevice area (A_w), single metastable pitting activity is the source for initiation of crevice corrosion, which later the crevice corrosion propagates.

The study by Suleiman et al.[24] supports the model proposed by Stockert and Bohni[23], where the authors found that the potential for crevice corrosion initiation on a sample covered with rust, is the same as metastable pitting on a sample without rust. The authors study the behaviour of pitting on a 304L stainless steel cover with rust. The authors stated that the rust

layer act as a crevice that undergoes the anion-selective process and local acidification, and thus prevents or delays the re-passivation process of metastable pits.

Laycock et al.[18] tested each theory; passive dissolution, IR drop, inclusion dissolution, and metastable pitting, in their study of crevice corrosion initiation in stainless steels, and they concluded that metastable pitting theory fits the best with their study. The authors measured metastable pits occurred with respect to temperature, for 904 L stainless steel. They found that metastable pits occurred even at a temperature lower than the CCT value, beginning from 0 ^{o}C. CCT value for the steel they are studying, 904 L is 15-20 ^{o}C. By taking into account the statement by Stockert and Bohni[23], where there is an average number of metastable pits occurred before the initiation of crevice corrosion, and assuming the rate of metastable pitting rates is independent of time. The authors stated that crevice corrosion might initiate at a temperature lower than CCT but require a longer time. As for crevice corrosion to initiate at 2 ^{o}C, it needs 5-10 times longer time compared to the initiation time of crevice corrosion at 20 ^{o}C. The authors concluded his work that metastable pitting is the reason for the initiation of crevice corrosion.

2.2 Reaction in Crevice Corrosion

Electrochemical reactions of species involved in crevice corrosion are listed in Table 2-1. Based on four stage[1,14] mechanisms, if a metal is placed in near-neutral saltwater, initially metal dissolution (reaction 1) and oxygen reduction (reaction 2) occurred uniformly inside and outside of the crevice. As oxygen depletes inside the crevice, metal undergoes hydrolysis (reactions 6 & 7).

Table 2- 1: Electrochemical and chemical reaction in crevice corrosion.

No.	Reaction / Chemical Equation / Equilibrium Potential (V_{SHE}), T=25 °C	The equation used in the model.
1	Metal dissolution $M\,(s) \rightarrow\ M^{n+}(aq) + ne^-$	Yes
2	Oxygen reduction (neutral/alkaline condition) $O_2 + 2H_2O + 4e^- \rightarrow 4OH^-$ $E = 0.401 + 0.0148 \log P_{O_2} - 0.0591 \log[OH]$	Yes
3	Hydrogen reduction (neutral/alkaline condition) $2H_2O + 2e^- \rightarrow H_2 + 2OH^-$ $E = -0.828 - 0.0591 \log[OH^-] - 0.0295 \log P_{H_2}$	Yes
4	Oxygen reduction (acidic condition) $O_2 + 4H^+ + 4e^- \rightarrow 2H_2O$ $E = 1.228 - 0.0591\ pH + 0.0148 \log P_{O_2}$	Yes
5	Metal ion hydrolysis $M^{n+} +\ H_2O \rightarrow M(OH)^{(n-1)+} + H^+$	Yes
6	Precipitation of hydroxide $M(OH)^+ + H_2O \leftrightarrow M(OH)_2(s) + H^+$	Yes
7	Hydrogen reduction (acidic condition) $2H^+ + 2e^- \rightarrow H_2$ $E = 0.0 - 0.0591\ pH - 0.0295 \log P_{H_2}$	Yes
8	Chlorine reduction $Cl_2 + 2e^- \rightarrow 2Cl^-$ $E = 1.358 - 0.0295 \log P_{cl_2} - 0.0591 \log[Cl^-]$	yes
9	Dissociation of water $H_2O\ \leftrightarrow\ H^+ + OH^-$	yes
10	Additional reaction in chloride $M^{2+} + Cl^- \leftrightarrow\ MCl^+$ $MCl^+ + Cl^- \leftrightarrow\ MCl_2$	yes
11	Hypochlorous acid reduction (neutral condition) $HClO +\ H^+ + 2e^- \rightarrow\ H_2O +\ Cl^-$ $E = 1.494 - 0.0295\ pH + 0.0295 \log[HClO] - 0.0295 \log[Cl^-]$	no
12	Hypochlorite reduction (alkaline condition) $ClO^- + H_2O + 2e^- \rightarrow 2OH^- + Cl^-$ $E = 0.890 + 0.0295 \log[ClO] - 0.0591 \log[OH^-] - 0.0295 \log\,[Cl^-]$	no
13	Sulphur reduction $S + 2H^+ + 2e^- \rightarrow H_2S$ $E = 0.141 - 0.0591\ pH - 0.0295 \log P_{H_2S}$	no
14	Thiosulphate reduction $S_2O_3{}^{2-} + 6H^+ + 4e^- \rightarrow 2S + 3H_2O$ $E = 0.499 - 0.0887\ pH + 0.0148 \log[S_2O_3]$	no

2.3 Crevice Corrosion Models

A transient model provides information on time and concentration changes in the crevice. There are four models discussed in this subchapter, which are Oldfield & Sutton model, Sharland model, Walton model, and Watson model.

Oldfield & Sutton Model

Oldfield and Sutton[14] developed a transient model to predict several parameters during the initiation of crevice corrosion in stainless steels in a 1M sodium chloride solution. This model is based on infinitely dilute solution and electroneutrality theory. It is assumed that mass transport only occurred between the crevice and bulk solution. It is assumed that migration is the transport of a current and it was carried by alloy ions, sodium cation (Na^+), and chloride ions (Cl^-). It also assumed that the diffusion coefficients for all species are the same. The model follows a four-stage mechanism[1,14] and is thus modelled accordingly based on the first three stages, which are; (i) deoxygenation in crevice solution, (ii) metal hydrolysis, and decrease in pH, (iii) breakdown of the passive film and critical crevice solution. This model predicted the initiation time and the comparison agreed with his experimental data.

In the first stage where the consumption rate of oxygen inside the crevice is higher than oxygen diffusion into the crevice cause depletion of oxygen in the crevice solution. The authors estimate the time taken for oxygen to deplete inside the crevice, t_d, and the distance at which oxygen can diffuse during the depletion time,δ_d by using equations (13) and (14), respectively.

$$t_d = \frac{n\,F\,c_{o2}\,x}{i_p} \tag{13}$$

$$\delta_d = (\pi D t_d)^{0.5} \tag{14}$$

Where n is a number of equivalents per mol of oxygen reduction (mol), F is Faraday constant (dimensionless), C_{o2} is the initial concentration of oxygen in ($mol.cm^{-3}$), x is average crevice gap (cm), i_p, is passive current in ($\mu A.cm^{-2}$), D is diffusion coefficient for oxygen ($m^2.s^{-1}$).

The authors stated that both parameters, t_d, and δ_d were being used to determine minimum crevice depth. Oxygen depletion occurs when the minimum crevice depth is exceeded. In addition, the time taken for oxygen depletion is much shorter to be compared with the overall time of crevice corrosion.

In the second stage where metal hydrolyses, the concentration of chemical species changes, the formation of hydrogen ions increases, and pH in the crevice fall. Three chemical species included in this model are Fe^{2+}, Cr^{3+}, $Ni^{2+}$and Mo^{3+}. In this stage, the authors would like to estimate the time taken for pH fall, from initial pH in bulk concentration to critical pH. The authors use equation (15) to determine the time for pH drop with small steps of ΔpH.

$$t(pH \rightarrow pH - \Delta pH) = \frac{[Cr]_T}{R(Cr)} \quad (15)$$

Where $[Cr]_T$ is the total amount of chromium that enters the crevice (mol) and $R(Cr)$ is the rate of production of chromium ions (mol.s^{-1}).

In the third stage, passive film breakdown and CCS are responsible for rapid crevice corrosion. The authors stated that based on pH-time variations shown in their work, and with a known value of CCS, they were able to predict if breakdown will occur and the time taken for its breakdown.

Assumptions used in the Oldfield and Sutton model are that diffusion coefficients for all species are the same, the region of mass transport taken into account is in between crevice and bulk solution and sodium cation (Na^+), and chloride ions (Cl^-) in the solution act as the carrier for current. Oldfield and Sutton's model follows a four-stage mechanism[1,14] and thus modelled accordingly based on the first three stages, which are:

(i) Deoxygenation in crevice solution, where equation (13) is used to estimate the time taken for oxygen to deplete inside the crevice,t_d, and equation (14) is used to calculate the distance which oxygen can diffuse during the depletion time,δ_d.

(ii) Metal hydrolysis and decrease in pH, where the authors use equation (15) to calculate the time of pH drop with small steps of ΔpH.

(iii) Referring to the pH-time variation and known critical crevice solution (CCS) value, the authors can predict if a breakdown of the passive film will occur.

Sharland Model

Sharland and Tasker[25] developed a model to study the propagation of crevice and pitting corrosion of carbon steel in dilute sodium chloride solution. It is a steady-state model based on dilute solution theory and electroneutrality. The model includes diffusion, migration, and chemical and electrochemical reactions as equation (16). It is assumed that no convection presence due to the crevice's geometry and diffusion coefficient of all species are the same except H^+ and OH^-.

$$D_i\left[\frac{d^2C_i}{dx^2}+\frac{z_i}{RT}\frac{d}{dx}\left(c_i\frac{d\emptyset}{dx}\right)\right]+R_i=0 \qquad (16)$$

There are six chemical species included in the model which are Fe^{2+}, $FeOH^+$, H^+, OH^-, Na^+ and Cl^-. Electrochemical and chemical processes included are listed in Table 2- 2. The model shows that the concentration of metal ions (Fe^{2+}), hydrogen ions (H^+), and chloride ions (Cl^-) increases in the pit. In addition, those concentrations increase with higher potential applied. One of the limitations of this model is the generic diffusion coefficient.

Later, Sharland[26] developed another model to predict the induction period of crevice corrosion in stainless steel. This model is based on a four-stage mechanism[1,14] with the assumption that it is deoxygenated inside the crevice and hydrogen reduction within the crevice is negligible. This model follows ion production within the crevice, mass transport of ions, and chemical equilibrium. Mass transport is based on infinitely dilute solution theory and includes diffusion, migration, and chemical reaction. Convection is neglected in mass transport due to its narrow geometric. Sharland's later model is expressed in equations (17) and (18).

$$\frac{\partial c_i}{\partial t}=D_i\left[\frac{\partial C_i}{dx^2}+z_iU_i\frac{d}{dx}\left(c_i\frac{d\emptyset}{dx}\right)\right]+R_i \qquad (17)$$

$$U_i = \frac{D_i}{R\,T} \tag{18}$$

Sharland model was simulated based on the data from Alavi and Cottis experiment[27] and Sharland model predicted the potential drop and pH close to the experimental data from Alavi and Cottis experiment[27]. Simulated potential drop within crevice at 90 hours is 8 mV and experimental potential drop is 6-9 mV, for corrosion current density, i_L of 10^{-3} A.m^{-2}. However, at a corrosion current density,i_L of 10^{-2} A.m^{-2}, the simulated potential drop is 68 mV, way too high than the experimental value (6-9 mV). There was no corrosion current density measured in Alavi and Cotti's experiment, therefore three values of corrosion current density; 10^{-3},10^{-2},10^{-1} A.m^{-2} were assumed in their model.

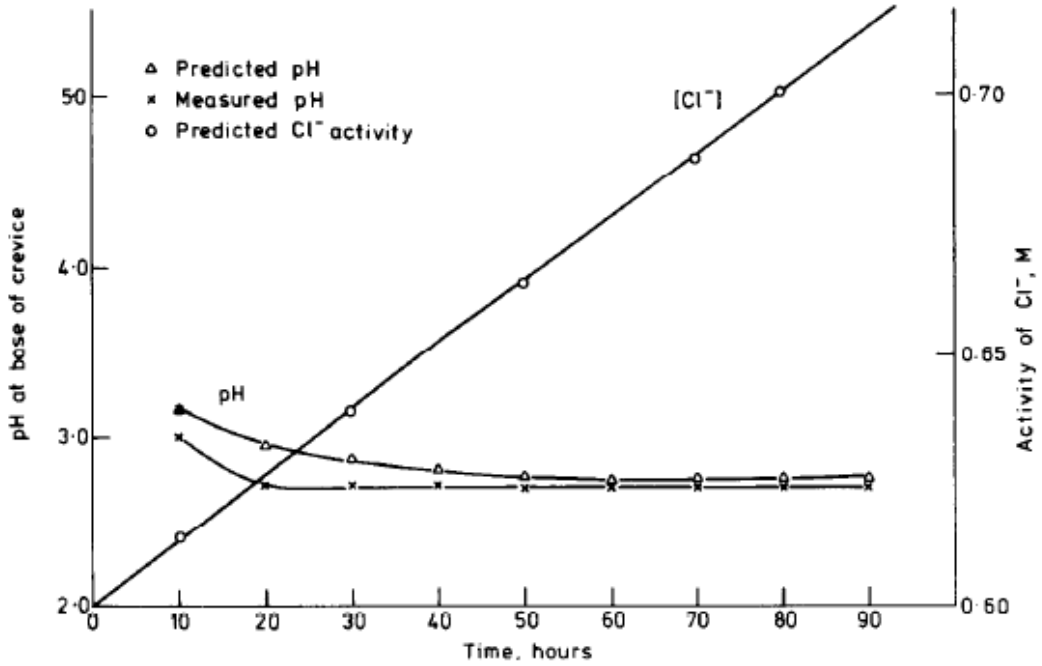

Fig.2- 3: Comparison of measured and predicted pH at the bottom of crevice, with current density of 10^{-2} A.m^{-2}.

In addition to that, the model predicted closely with measured experiment pH at the base of a crevice. Both show that pH at the base of the crevice decreases with time, but reaches a steady state after 20 hours, as shown in Fig. 2-3. Although it is predicted that chloride concentration in the crevice increases with time but that was not the result obtained in the experiment, most probably due to the wider gap of the crevice.

Table 2- 2: Electrochemical and chemical reaction based on Sharland Model.

Electrochemical reaction	**Chemical reaction**
Metal dissolution: $\mathbf{Fe \rightarrow Fe^{2+} + 2e^-}$	Water dissociation: $H_2O \leftrightarrow H^+ + OH^-$
Water reduction: $\mathbf{H_2O + e^- \rightarrow H^+ + OH^-}$	Metal hydrolysis: $Fe^{2+} + H_2O \leftrightarrow FeOH^+ + H^+$
Hydrogen reduction: $\mathbf{2H^+ + 2e^- \rightarrow H_2}$	

Walton Model

Walton[28] developed a one-dimensional steady-state model to evaluate the transport process and reactions within crevices and pits. It is based on the infinitely dilute solution theory and electroneutrality equation. In this model, the author assumed that, no changes in concentration at the crevice mouth. The author used mass transport, which includes diffusion and migration, as shown in (19).

$$J_i = -nD_i\nabla C_i - \frac{n\, z_i\, D_i\, F}{R\, T} C_i \nabla \emptyset_s \qquad (19)$$

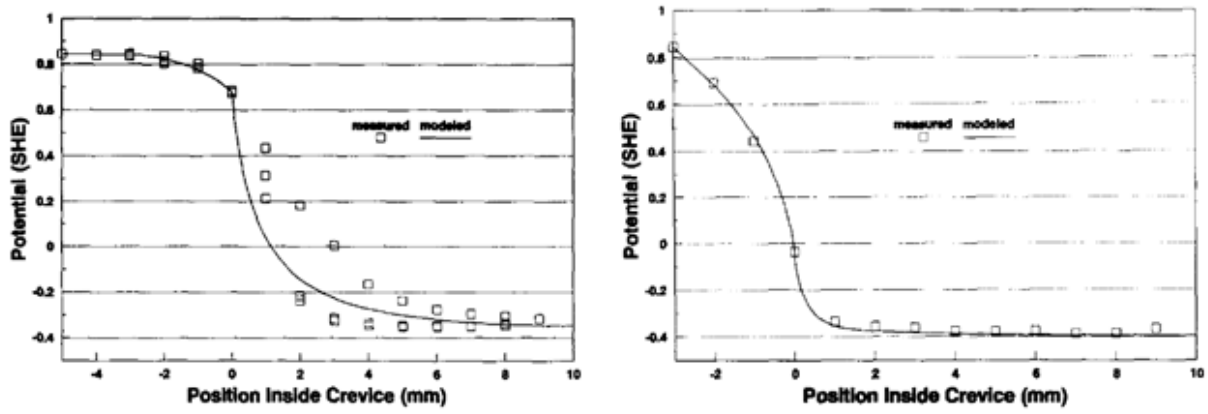

Fig.2- 4: Simulated potential by Walton model closely predicted the measured potential in the experiment by Valdes-Mouldon. [28]

The author included electrochemical reactions; metal dissolution and hydrogen evolution at the metal-solution interface and chemical reaction; metal hydrolysis. This model was used to simulate an experiment by Valdes-Mouldon and the model predicts closely the measured potential inside and outside of the crevice as shown in Fig. 2-4.

Later, Walton[29] et al. developed a transient numerical model for crevice corrosion. The model is based on the infinity dilute solution and electroneutrality equation. It is based on the Nernst-Planck equation, which considers diffusion and migration but neglects convection. Equation (20) shows the flux of aqueous chemical species.

$$N_n = \frac{-D_n C_n}{RT} \nabla \mu_n = -\frac{D_n C_n}{RT} \nabla(\mu + z_n F \emptyset_s) \qquad (20)$$

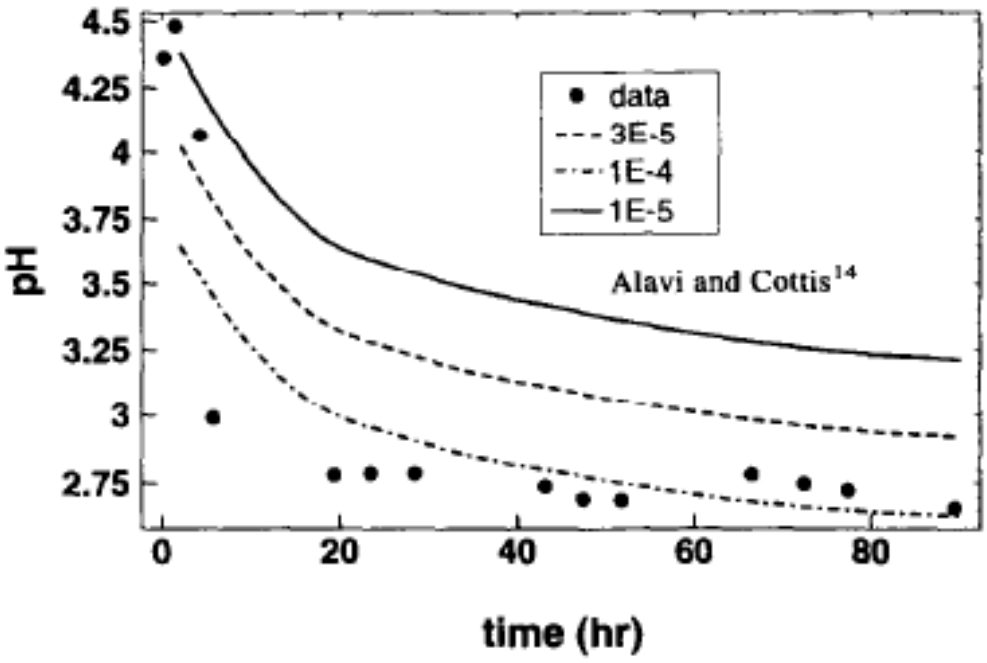

Fig.2- 5: Simulated result based on Walton[29] model and verified by Alavi and Cottis[27] experiment, at various anodic current densities.

The model was verified by Alavi and Cottis[27] in an experiment, which assumed that reactions occur at the metal–solution interface and thirteen reactions were involved. The model was run for 90 hours and one of the main results with respect to time is shown in Fig. 2-5.

Watson Model

Watson and Postlethwaite[30] developed a transient model to estimate the incubation time for active crevice corrosion to occur and simulate the concentration of metal species in the crevice solution. The authors developed the model based on infinitely dilute solution theory and the Poisson equation. Equation (21) is the equation used in the authors' model. The

$$\frac{\partial C_i}{\partial t} = -\frac{z_i u_i F^2 c_i}{\varepsilon}\sum_{j=1}^{n} z_j c_j - \frac{z_i u_i \nabla c_i}{F\sum_{j=1}^{n} z_j^2 u_j c_j} i - \frac{z_i u_i \nabla c_i}{F\sum_{j=1}^{n} z_j^2 u_j c_j}\sum_{j=1}^{n} z_j D_j \nabla_{cj} + D_i \nabla^2 c_i + R_i \quad (21)$$

With indication of,

$-\frac{z_i u_i F^2 c_i}{\varepsilon}\sum_{j=1}^{n} z_j c_j$	Poisson term
$-\frac{z_i u_i \nabla c_i}{F\sum_{j=1}^{n} z_j^2 u_j c_j} i$	1st migration term
$-\frac{z_i u_i \nabla c_i}{F\sum_{j=1}^{n} z_j^2 u_j c_j}\sum_{j=1}^{n} z_j D_j \nabla_{cj}$	2nd migration term
$+D_i \nabla^2 c_i$	Diffusion term
R_i	Reaction term

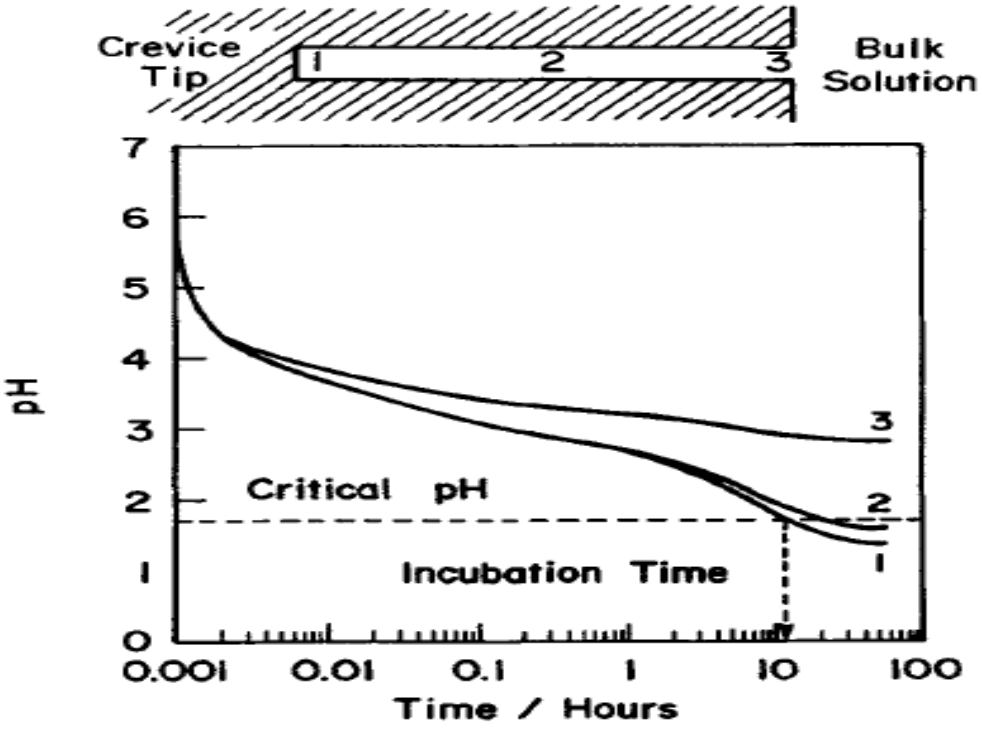

Fig.2- 6: Result from the Watson model: pH within crevice decrease with time.

The result of their model labeled 1, 2, and 3 represents cells at the tip of a crevice, middle of the crevice, and mouth of the crevice, respectively. Fig.2-6 shows pH in crevice solution decreases with time and incubation time of approx. 10 hours. In addition, pH at the crevice tip is lower than in the crevice mouth, which probably means active corrosion at the bottom of the crevice and a passive state at the crevice mouth.

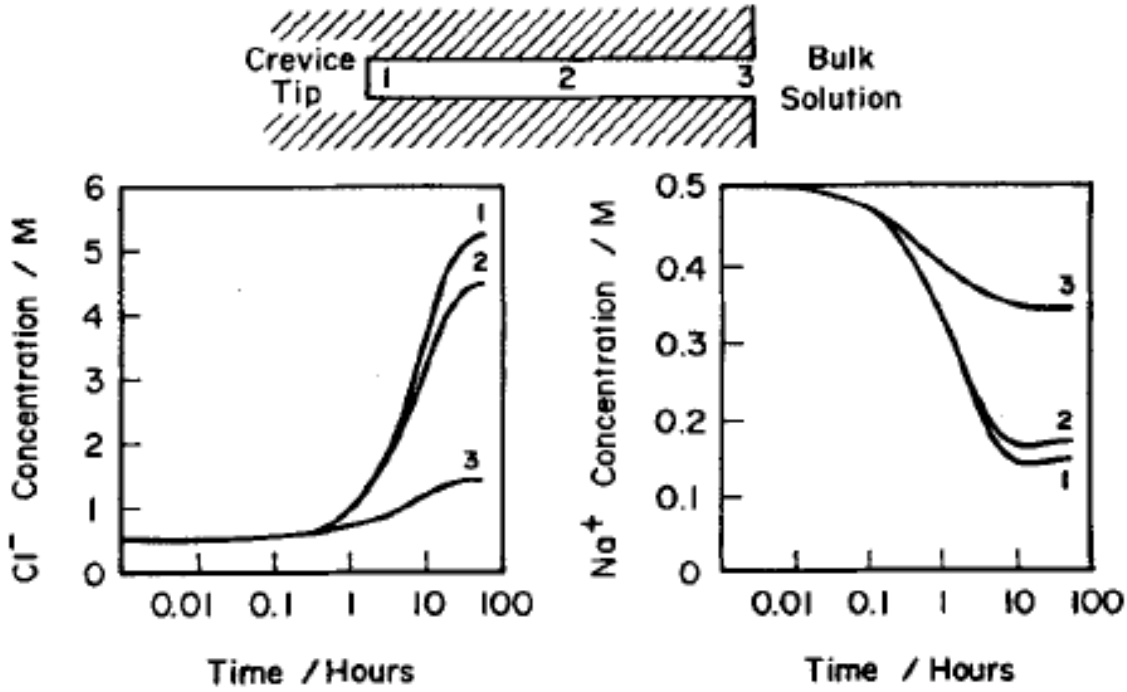

Fig.2- 7: Results from Watson model: chloride concentration within crevice increases with time.

Fig. 2-7 shows that the concentration of chloride ions inside the crevice (tip and middle of crevice) is higher compared to bulk concentration (crevice mouth). The concentration of chloride starts to increase after approx. 1 hour when chloride ions start to diffuse into the crevice to compensate for increased concentration of metal ions.

The authors also simulated the concentration of ferrous, nickel, chromium, and nickel species with respect to time. They also simulated the influence of crevice geometry (crevice depth and gap) on incubation time. In general, the model has general agreement with results from other literature.

This model follows the model developed by Sharland and Tasker[25] that takes into account convection, diffusion, migration, chemical, and electrochemical reaction equation. Sharland and Tasker[25] developed a model to study crevice propagation in diluted salt solution and includes diffusion, migration, chemical, and electrochemical reaction as equations. Meanwhile, the model by Walton[28] assumed that there are no concentration changes at the crevice mouth. The model developed by Watson and Postlethwaite[30] is based on the infinitely dilute solution theory. The model developed by Oldfield and Sutton[14] is based on three out of four stages of crevice corrosion mechanisms; (i) crevice deoxygenation, (ii) metal hydrolysis, and (iii) breakdown of the passive film and critical crevice solution.

There are four theories of crevice corrosion initiation discussed in this chapter which are passive dissolution theory, IR drop theory, inclusion dissolution theory, and metastable pitting theory. Four models discussed in this chapter are Oldfield & Sutton model, the Sharland model, the Walton model and the Watson model. This research work is an extension of previous works by simulating a practical (nut and bolt) geometry, compared to a straight line geometry in previous works. This research work fills in the gap in Oldfield & Sutton model by providing the data and visualizing the pH, potential, current density, and oxygen concentration with respect to time or position. In addition to that, this research work provides a new investigation on the relationship between crevice width and oxygen concentration hence the corrosion kinetics.

3.0 Methodology

3.1 COMSOL Multiphysics

Finite Element Methods (FEM) divides the problems into smaller sections and estimate the solution based on the partial differential equation. During the developmental stage, FEM is categorised into discretisation, approximation, and assembly stages. In the discretisation stage, grids of finite elements are generated and the size of the grid influences the accuracy of the model. In the approximation stage, each element is defined approximately and one calculated value depends on another value in the system by approximation. In the assembly stage, equations for each element are assembled to build a global equation system.

COMSOL Multiphysics is one of the reputable software built for finite element analysis and simulation. It is designed to solve physics phenomena simultaneously, either conventional physic interfaces or partial differential equations. It also has corrosion and electrochemistry modules which are beneficial to investigate corrosion processes. Nernst-Planck equations were used in the model to solve electrochemical questions, which includes convection, diffusion, and migration transport phenomenon.

3.2 Crevice Geometry

Firstly, a geometry that represents the crevice of iron nut and bolt was designed in Comsol software and the dimension is shown in fig. 3-1 and fig. 3-2. There are 2 geometries in this work and the main difference is the depth of the crevice. Geometry 1 is a depth of 10 mm as shown in fig 3-1 and Geometry 2 has a depth of 20 mm as shown in fig. 3-2.

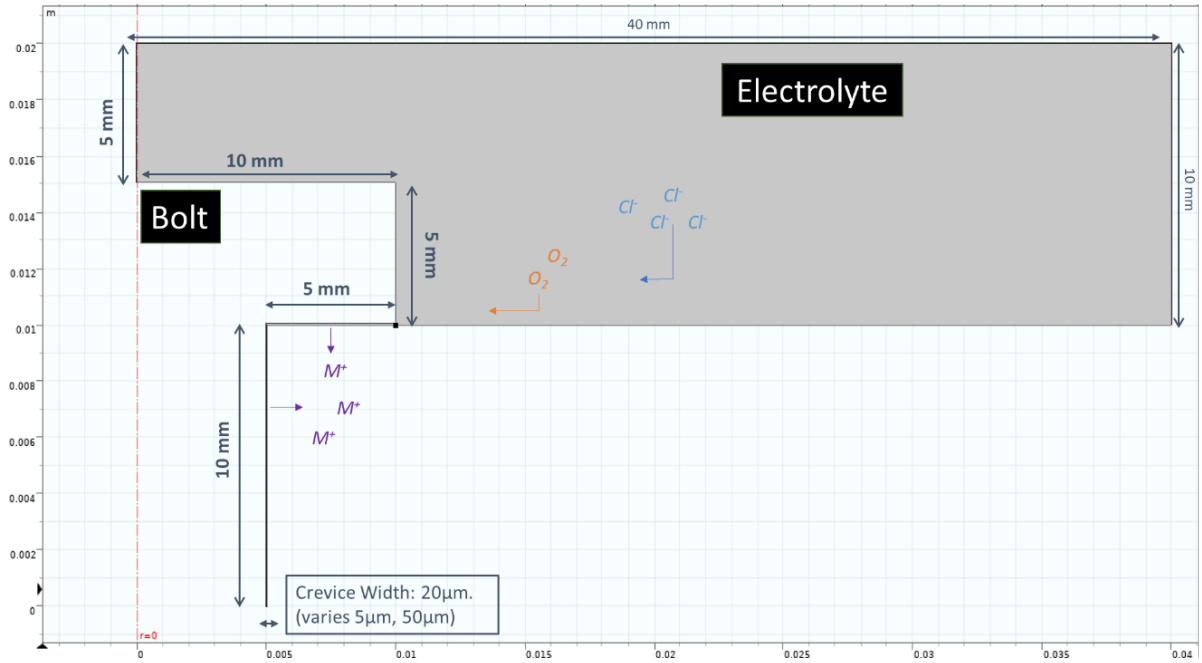

Fig.3- 1: Dimension of Geometry 1, with the crevice depth of 10mm. Crevice width was varied at 5µm, 20µm, and 50µm. It is shown in the figure, metal is undergoing metal dissolution producing metal ions, (M^+), meanwhile, oxygen (O_2) and chloride (Cl^-) ions diffuse into the crevice.

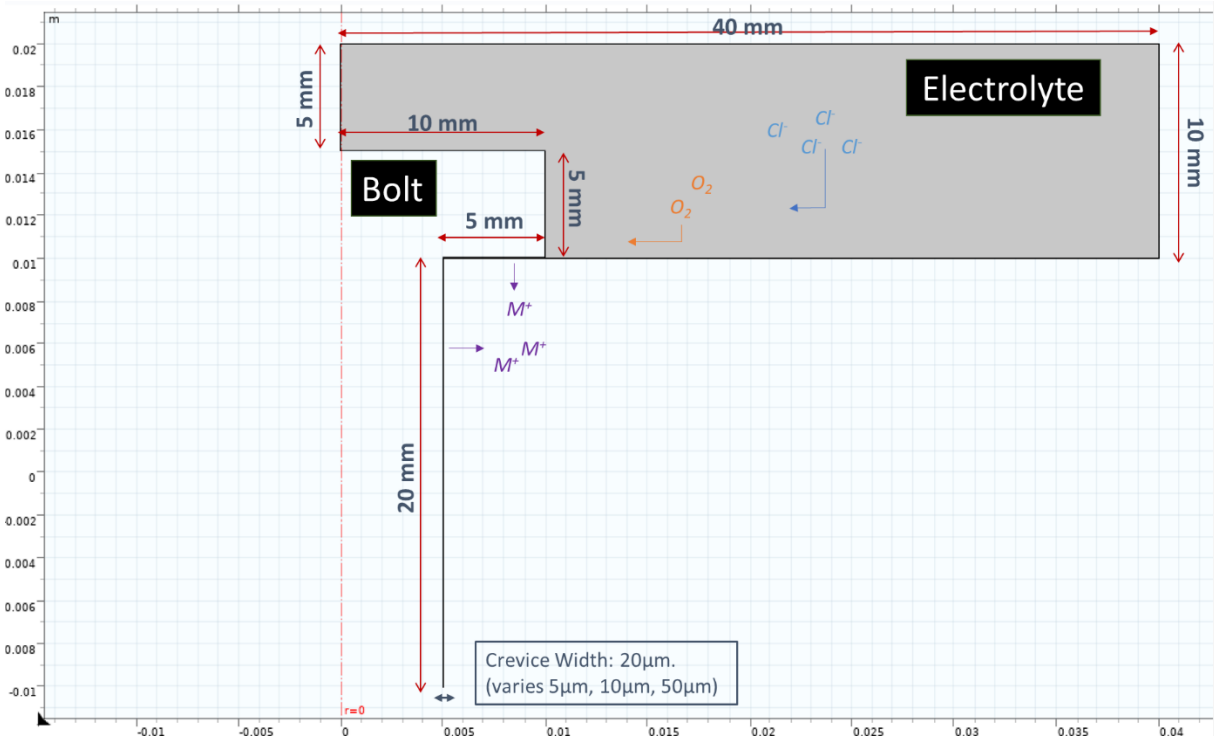

Fig.3- 2: Dimension of Geometry 2, with crevice depth of 20mm. Crevice width was varied at 5µm, 10µm, 20µm, and 50µm. It is shown in the figure, metal is undergoing metal dissolution producing metal ions (M^+) and meanwhile, oxygen (O_2) and chloride (Cl^-) ions diffuse into the crevice.

3.3 Meshing

Secondly, based on the infinite element method and to simulate the designated geometry, meshing is required. Meshing is user-defined and the parameters used in meshing are divided into 3 subdivisions of general size, edge, and free-triangular. Details of the size of mesh defined in this model for both geometries are listed in table 3-1. Fig. 3-2 represents the meshing in Geometry 1, where the maximum size of each element is 2 mm and 0.4 μm.

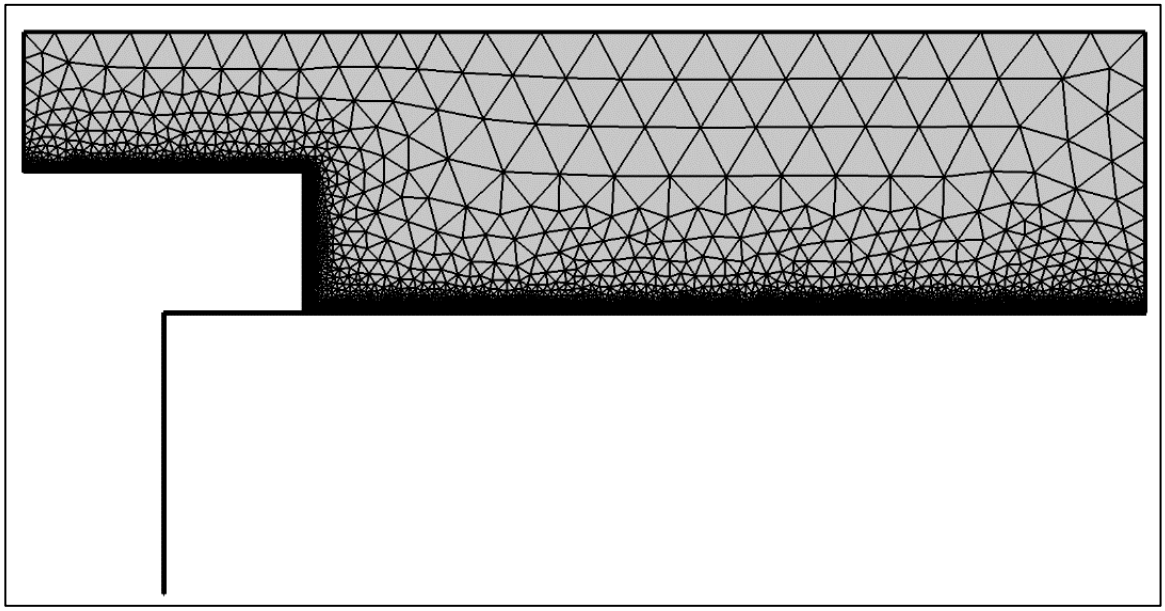

Fig.3- 3: Meshing of Geometry 1. Maximum element size was 2 mm and the minimum element size was 0.4 μm. Details of meshing parameters can be found in Table 3-1.

Table 3- 1: Values and parameters used for meshing (Geometry 1 & 2)

General size	
Maximum element size:	2 mm
Minimum element size:	0.4 μm
Maximum element growth rate:	1.3
Curvature factor:	0.2
Resolution of narrow regions:	5
Edge	
Mesh inside crevice:	1.5 μm
Mesh outside crevice:	50 μm
Free Triangular	
Maximum element size:	1 mm
Minimum element size:	1 μm
Maximum element growth rate:	1.3

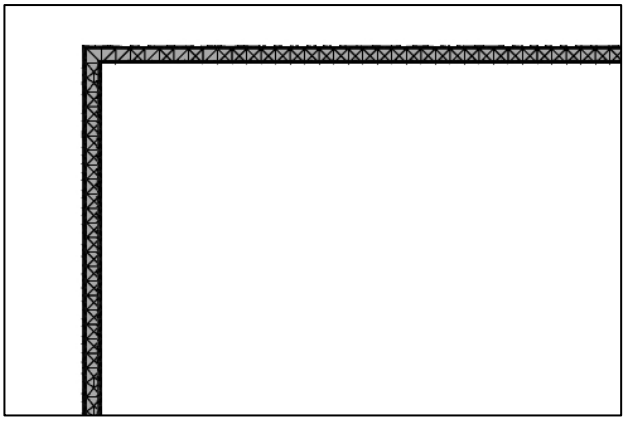

Fig.3- 4: Meshing inside the crevice, where minimum mesh size is 0.4µm and mesh size at the edge is 1.5µm. Details of meshing parameters can be found in Table 3-1.

3.4 Positions

Thirdly, four designated positions on the geometry were determined. Four 'probes' (pH-probe or oxygen-concentration-probe) were placed in these positions. There are 4 probes or points that are used in this model to monitor the behaviour inside of the crevice and outside of the crevice. Inside the crevice, there are 2 probes named "bottom of crevice" and "middle of crevice". Similarly, there are 2 probes outside of the crevice, named "mouth of crevice" and "outer edge". The locations of these probes are shown in Fig. 3-5. This research only focuses on iron dissolution and has not taken into account other metal dissolution such as nickel or chromium.

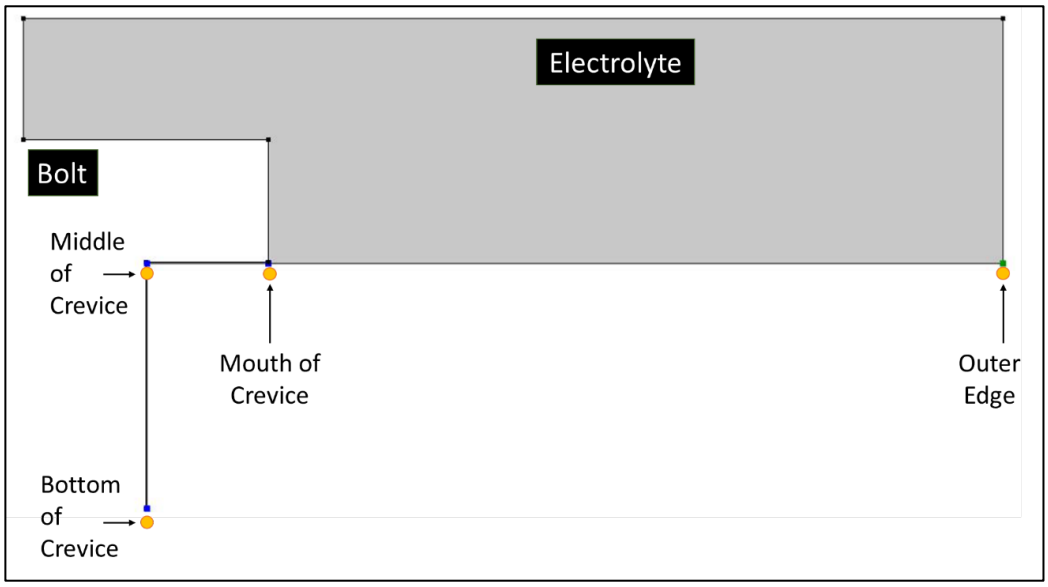

Fig.3- 5: Positions where virtual probes were placed within the crevice. In this thesis bottom and middle of the crevice are categorized as inside the crevice. Meanwhile mouth of the crevice and outer edge are categorized as outside of the crevice.

3.5 Simulations

Fourth, a simulation study was performed in Comsol software. Firstly to investigate the influence of solution ionic strength on the pH and potential inside and outside of the crevice, NaCl concentration was varied at 10M, 1M, 0.1M, and 0.01M. Secondly, to investigate the relationship between the size of crevice width and depth of crevice to the oxygen concentration inside and outside of crevice, the crevice width varied from 5 μm, 10 μm, 20 μm to 50 μm. A study on the influence of ionic solution strength was performed on geometry 1 (crevice depth of 10mm). Meanwhile, a study on the influence of crevice width was performed on both geometries; geometry 1 and geometry 2 (crevice depth of 20mm).

3.6 Parameters

Key parameters and variables used in this research were obtained from the literature. All parameters listed in Table 3-2 were kept constant and only several parameters were varied depending on the study. In the study of the influence of solution ionic strength, NaCl concentration varied from 0.01M to 10M. In the study of the influence of crevice with, the crevice width was from 5 μm to 50 μm.

Table 3- 2: Parameters and variables used in the simulation (Geometry 1 & 2)

Description	**Abbreviations**	**Value**	**Unit**
Transfer coefficient of ferrous iron	aFe	1	
Transfer coefficient of ferric iron	aFe3	0.5	
Transfer coefficient of hydrogen	aH	0.5	
Transfer coefficient of water	aH2O	0.5	
Transfer coefficient of oxygen	aO2	0.5	
Concentration of chloride ions initial	c0Cl	0.01, 0.1, 1, 10	M
Concentration of ferrous iron	c0Fe	$1x10^{-6}$	$mol.m^{-3}$
Concentration of ferric iron	c0Fe3	$7.06x10^{-7}$	$mol.m^{-3}$
Concentration of iron chloride	c0FeCl	$6.92x10^{-6}$	$mol.m^{-3}$
Concentration of iron hydroxide	c0FeOH	$5x10^{-8}$	$mol.m^{-3}$

Concentration of hydrogen ions	c0H	$1x10^{-4}$	$mol.m^{-3}$
Concentration of hydrogen	c0H2	0	$mol.m^{-3}$
Concentration of sodium ions	c0Na	0.01, 0.1, 1, 10.	M
Concentration of oxygen	c0O2	0.25	$mol.m^{-3}$
Concentration of hydroxide	c0OH	$1x10^{-4}$	$mol.m^{-3}$
Constant of convection rate	ConvectionRateConst	$2x10^{-5}$	$m.s^{-1}$
Diffusion coefficient of Chloride	DCl	$1x10^{-9}$	$m^2.s^{-1}$
Diffusion coefficient of ferrous iron	DFe	$1x10^{-9}$	$m^2.s^{-1}$
Diffusion coefficient of ferric iron	DFe3	$1x10^{-9}$	$m^2.s^{-1}$
Diffusion coefficient of iron chloride	DFeCl	$1x10^{-9}$	$m^2.s^{-1}$
Diffusion coefficient of iron (II) chloride	DFeCl2	$8.6x10^{-10}$	$m^2.s^{-1}$
Diffusion coefficient of iron hydroxide	DFeOH	$1x10^{-9}$	$m^2.s^{-1}$
Diffusion coefficient of hydrogen ions	DH	$9.3x10^{-9}$	$m^2.s^{-1}$
Diffusion coefficient of hydrogen	DH2	$1x10^{-9}$	$m^2.s^{-1}$
Diffusion coefficient of sodium ions	DNa	$1x10^{-9}$	$m^2.s^{-1}$
Diffusion coefficient of oxygen	DO2	$1.4x10^{-9}$	$m^2.s^{-1}$
Diffusion coefficient of hydroxide	DOH	$5.3x10^{-9}$	$m^2.s^{-1}$
Exchange current density for oxidation of iron	i0Fe	$2.7x10^{11}$	$A.m^{-2}$
Exchange current density for reduction of ferrous iron	i0Fe3	$1.57x10^{-8}$	$m.A.mol^{-1}$
Exchange current density for reduction of water	i0H2O	$8x10^{10}$	$A.m^{-2}$
Exchange current density for reduction of oxygen	iO2lim	0.1	$A.m^{-2}$
Passive current	iPassive	0.0096485	$A.m^{-2}$
No of electrons in iron oxidation	nFe	2	

Table 3- 3: Parameters and variables used in the simulation (Geometry 1 & 2)

Description	Abbreviations	Value	Unit
Passive Flux	Passive_Flux	$5x10^{-8}$	$mol.m^{-2}.s^{-1}$
Scale of Passivity at final	PassiveFinalScale	0.05	
Passive rate	PassiveRate	1	
Scale of passivity	PassiveScale	0.05	
External potential of metal	Estart	-0.8	V
Width of crevice	crevicewidth	5, 10, 20, 50	?m
Faraday constant	F	96485	C.mol-1
Gas constant	Rate_C	8.3145	$J.mol^{-1}.K^{-1}$
Molar mass of iron	Atomic_Weight_Fe	0.0558	$kg.mol^{-1}$
Density of iron	rhoFe	7870	$kg.m^{-3}$
Density of iron chloride	rhoFeCl2s	3160	$kg.m^{-3}$
Temperature	Temp_K	298.15	K
Backward rate constant for ionization of water	kbWater	$1x10^{8}$	$m^{3}.s^{-1}.mol^{-1}$
Forward rate constant for ionization of water	kfWater	1	$mol.m^{-3}.s^{-1}$
Equilibrium constant for ionization of water	KWater	$1x10^{8}$	$mol^{2}.m^{-6}$
Backward rate constant for hydrolysis of ferrous ion	kbFe	$2x10^{5}$	$m^{3}.s^{-1}.mol^{-1}$
Forward rate constant for hydrolysis of ferrous ion	kfFe	1	s^{-1}
Equilibrium constant for ionization of ferrous ion	KFe	$5x10^{-6}$	$mol.m^{-3}$
Backward rate constant for hydrolysis of ferric ion	kbFe3	$1.007x10^{-24}$	$m^{9}.s^{-1}.mol^{-3}$
Backward rate constant for $FeCl_2$ formation	kbFeCl2s	$1x10^{-16}$	$m^{7}.s^{-1}.mol^{-2}$

Forward rate constant for $FeCl_2$ formation	kfFeCl2s	$3.645x10^{-5}$	$mol.m^{-2}.s^{-1}$
Forward rate constant for $FeCl_2$ formation	KFeCl	$6.92x10^{-4}$	$m^3.mol$
Forward rate constant for Fe^{3+} formation	KFe3	$9.93x10^{15}$	$m^{15}.mol^{-5}$
Forward rate constant for Fe^{3+} formation	kfFe3	$1x10^{-8}$	$m^{24}.s^{-1}.mol^{-8}$
Time scale	tscale	-4	
Minimum time scale	tscalemin	-4	
Henry's law constant	kH	$2x10^{-7}$	$m.A.mol^{-1}$
Exchange current density for reduction of oxygen	kO2	$4.2x10^{-5}$	$m.A.mol^{-1}$
Charge of chloride ions	zCl	-1	
Charge of ferrous iron	zFe	2	
Charge of ferric iron	zFe3	3	
Charge of ferric chloride	zFeCl	1	
Charge of iron hydroxide	zFeOH	1	
Charge of hydrogen ions	zH	1	
Charge of hydrogen	zH2	0	
Charge of sodium	zNa	1	
Charge of oxygen	zO2	0	
Charge of hydroxide	zOH	-1	

4.0 Simulation & discussion

4.1 Influence of solution ionic strength

The influence of solution ionic strength on the corrosion behaviour of iron was simulated on Geometry 1. This subchapter (4.1) explains the influence of four sodium chloride (NaCl) concentrations on the pH, potential, passivity, and corrosion rate. The NaCl concentration used in this study is 10M, 1M, 0.1M, and 0.01M with constant crevice width constant at 20 μm.

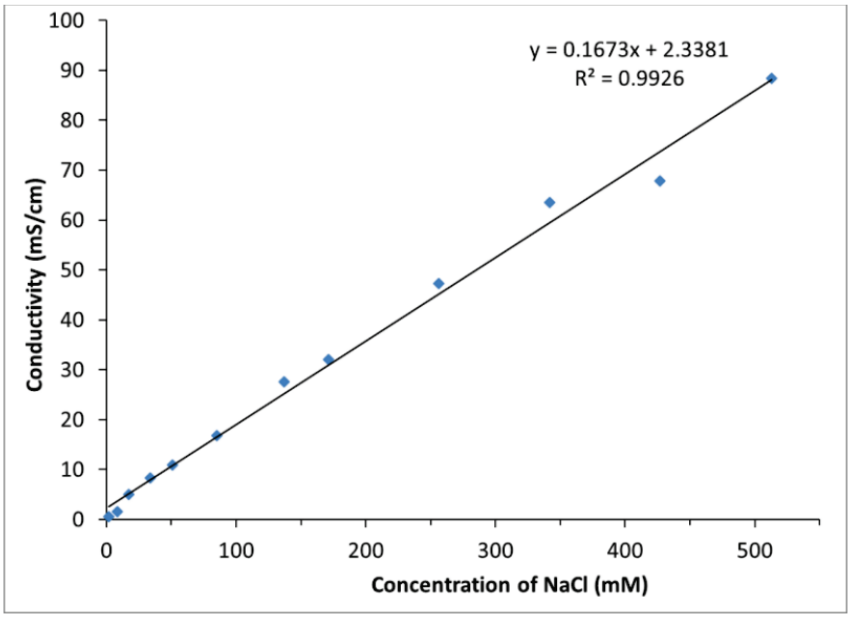

Fig. 4- 1: Plot of solution conductivity (mS.cm^{-1}) with NaCl concentration (mM).[33]

Fig. 4-1 is the plot of solution conductivity with respect to NaCl concentration. It shows the linear relation of solution conductivity with NaCl concentration.[33] The higher the concentration of NaCl solution, indicates there are more Na^+ and Cl^- ions in the liquid, hence increasing the migration of ions and resulting in a greater value of solution conductivity. Based on the linear relationship shown in Fig. 4-1, based on salt concentration, one can determine the solution conductivity. For 0.01M and 0.1M NaCl concentration, the solution conductivity are 4 mS.cm^{-1} and 19 mS.cm^{-1}, respectively. Meanwhile for 1M and 10M NaCl concentration, the solution conductivity are 0.17 S.cm^{-1} and 1.7 S.cm^{-1}, respectively.

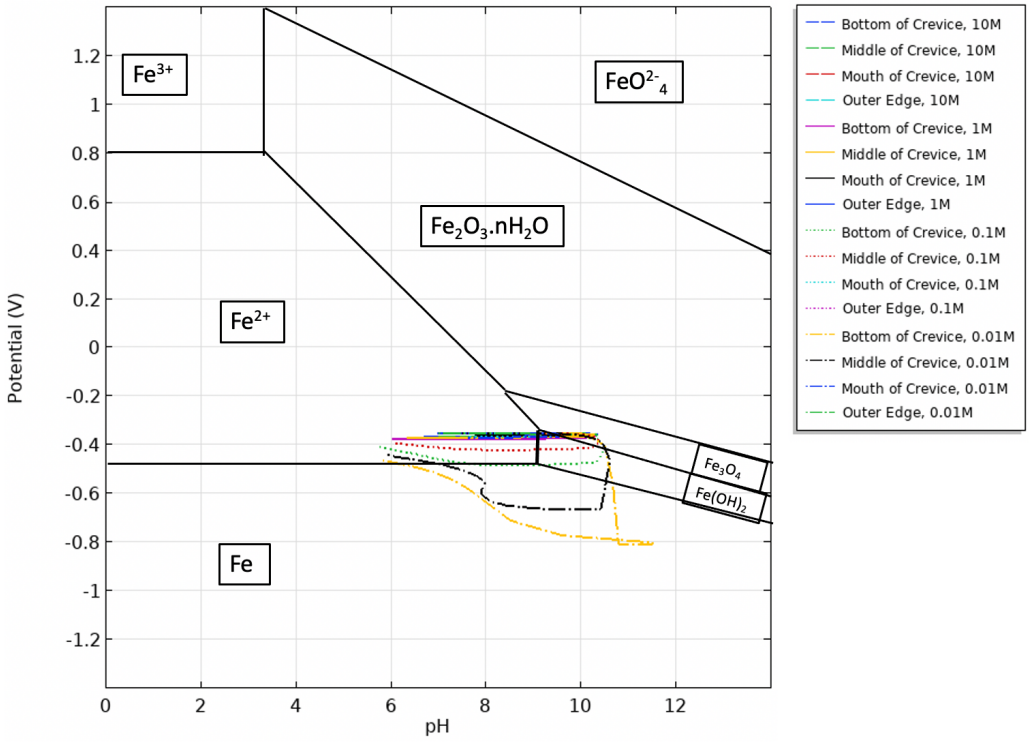

Fig. 4- 2: Pourbaix diagram of iron at all positions; outer edge, mouth, middle and bottom of crevice, in various ionic strength; 10M, 1M, 0.1M, and 0.01M. The result for 10M ionic strength is represented by a dashed line. The result for 1M is represented by a solid line. The result for 0.1M is represented by a dotted line. The result for 0.01M is represented by a dotted-dashed line.

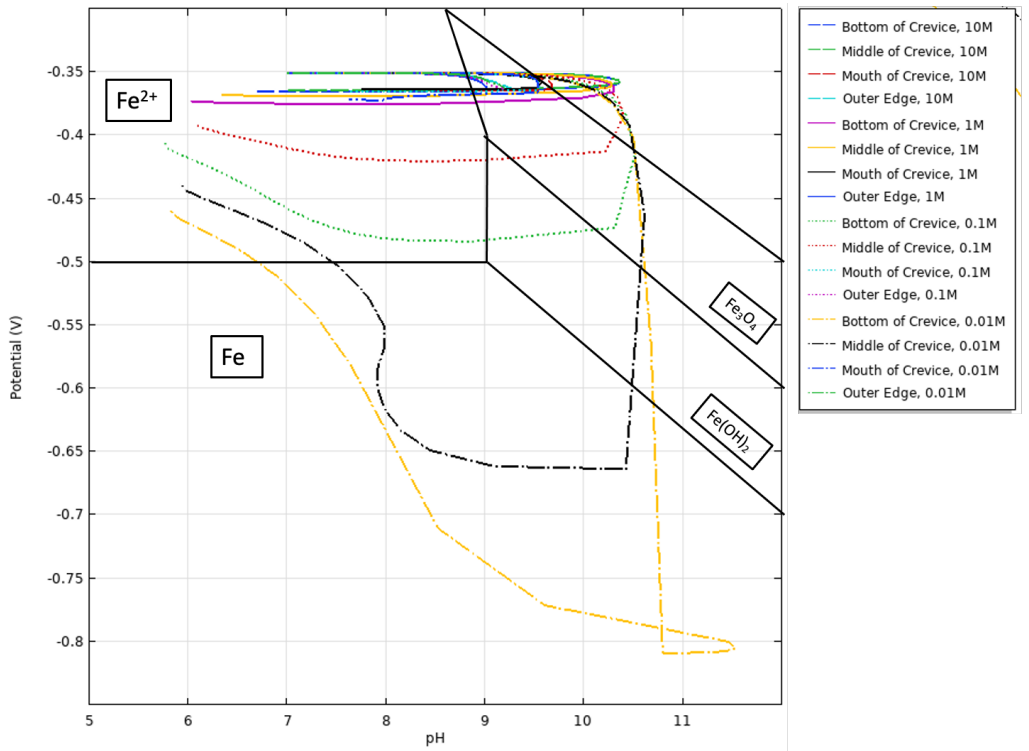

Fig. 4- 3: Magnified version of Fig. 4-2. Pourbaix diagram of iron at all positions; outer edge, mouth, middle and bottom of crevice, in various ionic strength; 10M, 1M, 0.1M, and 0.01M. The result for 10M ionic strength is represented by a dashed line. The result for 1M is represented by a solid line. The result for 0.1M is represented by a dotted line. The result for 0.01M is represented by a dotted-dashed line.

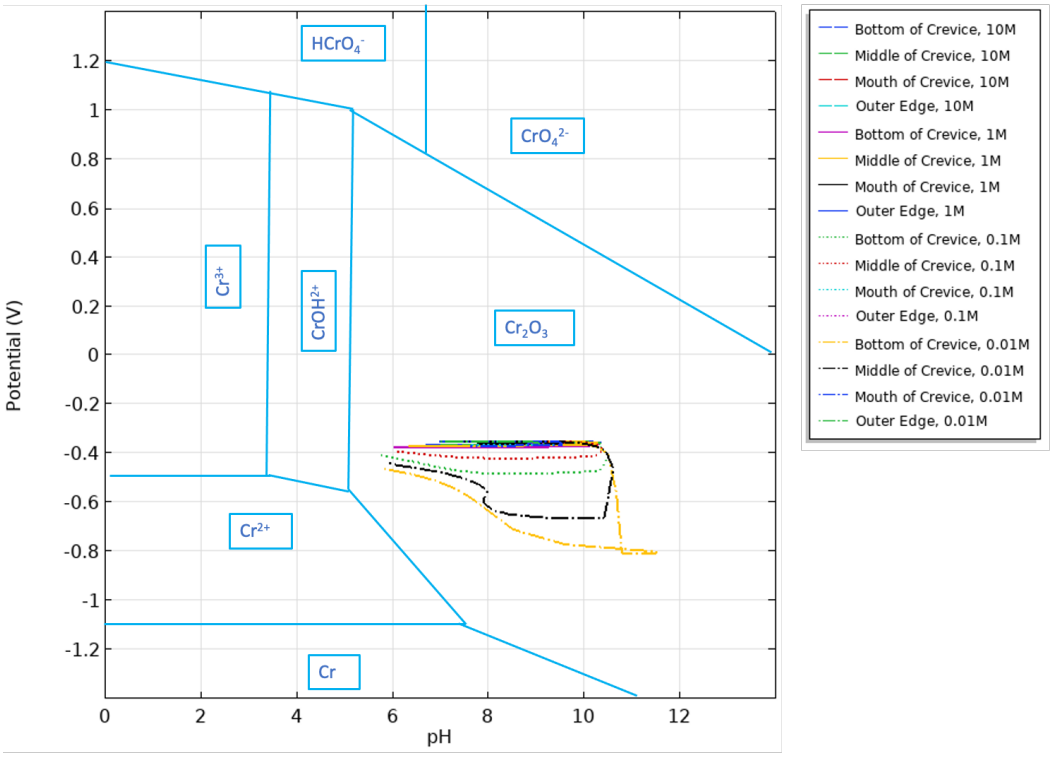

Fig. 4- 4: Pourbaix diagram of chromium at all positions; outer edge, mouth, middle and bottom of crevice, in various ionic strength; 10M, 1M, 0.1M, and 0.01M. The result for 10M ionic strength is represented by a dashed line. The result for 1M is represented by a solid line. The result for 0.1M is represented by a dotted line. The result for 0.01M is represented by a dotted-dashed line.

Fig. 4-2 and Fig.4-4 are the simulation of potential vs pH (pourbaix diagram) for all NaCl concentrations in all positions. The difference is that Fig.4-2 is the pourbaix diagram plot on pure iron and Fig.4-4 is the pourbaix diagram plot on pure chromium. Simulation in Fig.4-2 and Fig.4-3 are important to compare that metal made from pure iron will undergo metal dissolution compared to metal made from pure chromium. Fig. 4-3 is a magnified version of Fig.4-2. One can see from Fig. 4-3, where the green dotted line is a simulation at bottom of the crevice for 0.1M NaCl concentration. Meanwhile, the yellow dash-dotted line is a simulation at the same position (bottom of crevice) for 0.01M NaCl concentration. An in-depth explanation for each simulation, at each position (bottom of crevice, middle of crevice, mouth of crevice, outer edge) in each NaCl concentration (10M, 1M, 0.1M, 0.01M) and are explained more in detail below. Magnified simulation of potential vs pH (pourbaix diagram), pH vs time, and potential vs time, in each NaCl solution, are shown in the figures below. Simulation of potential vs pH or magnified pourbaix diagram for 10M NaCl concentration at various positions is shown in Fig. 4-5 and for 1M NaCl concentration is shown in Fig. 4-9.

Meanwhile magnified pourbaix diagram for 0.1M NaCl concentration at various positions is shown in Fig. 4-13 and a simulation of potential vs pH for 0.01M NaCl concentration is shown in Fig. 4-17. As shown in Fig. 4-2 and Fig. 4-4, metal made from pure iron will undergo active corrosion compared to metal made from pure chromium. These simulations validate the importance of chromium in the fabrication of alloy or stainless steel to prevent active corrosion. Chromium is needed because it provides a protection oxide layer on top of the iron metal and thus protects the iron metal beneath it from undergoing active corrosion.

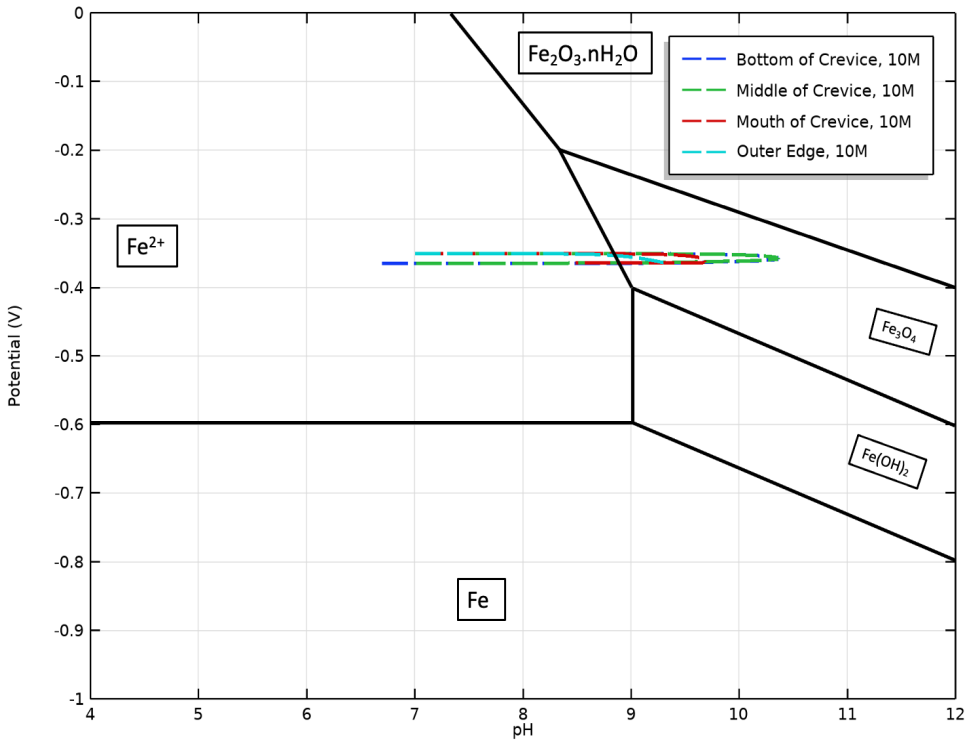

Fig. 4- 5: Pourbaix diagram of iron in 10M NaCl solution. The result for the 10M NaCl concentration study is represented by the dashed line. The blue dashed line represents the bottom of the crevice, the green dashed line represents the middle of the crevice, the red dashed line represents the mouth of the crevice and the cyan dashed line represents the outer edge.

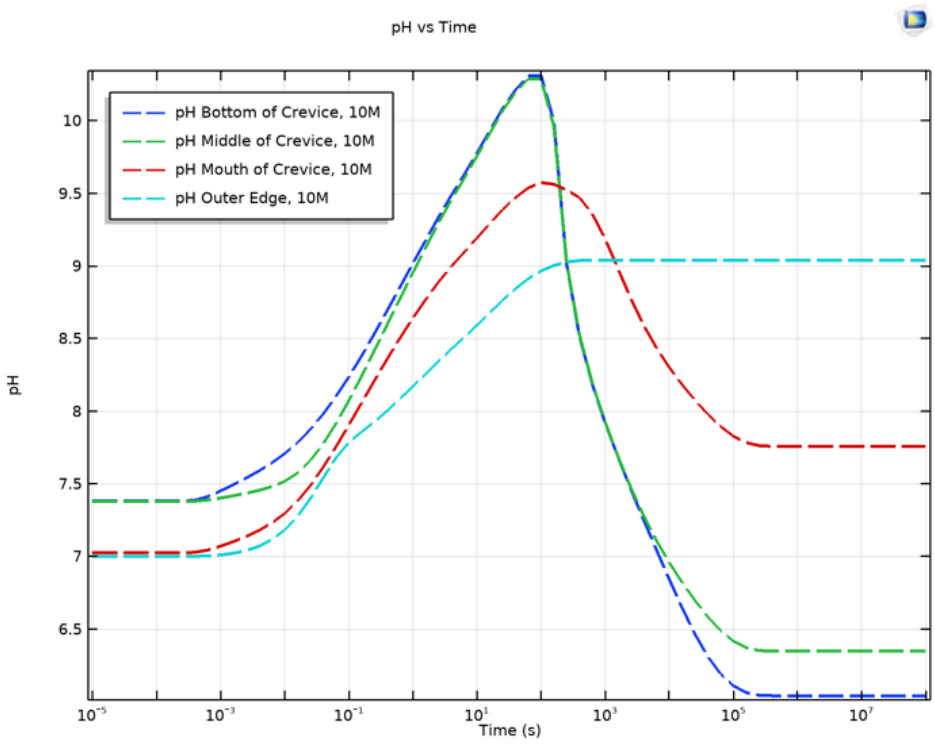

Fig. 4- 6: Simulation of pH as a function of time of iron in 10M NaCl solution. The result for 10M NaCl concentration represents by the dashed line. The blue dashed line represents the bottom of the crevice, the green dashed line represents the middle of the crevice, the red dashed line represents the mouth of the crevice and the cyan dashed line represents the outer edge.

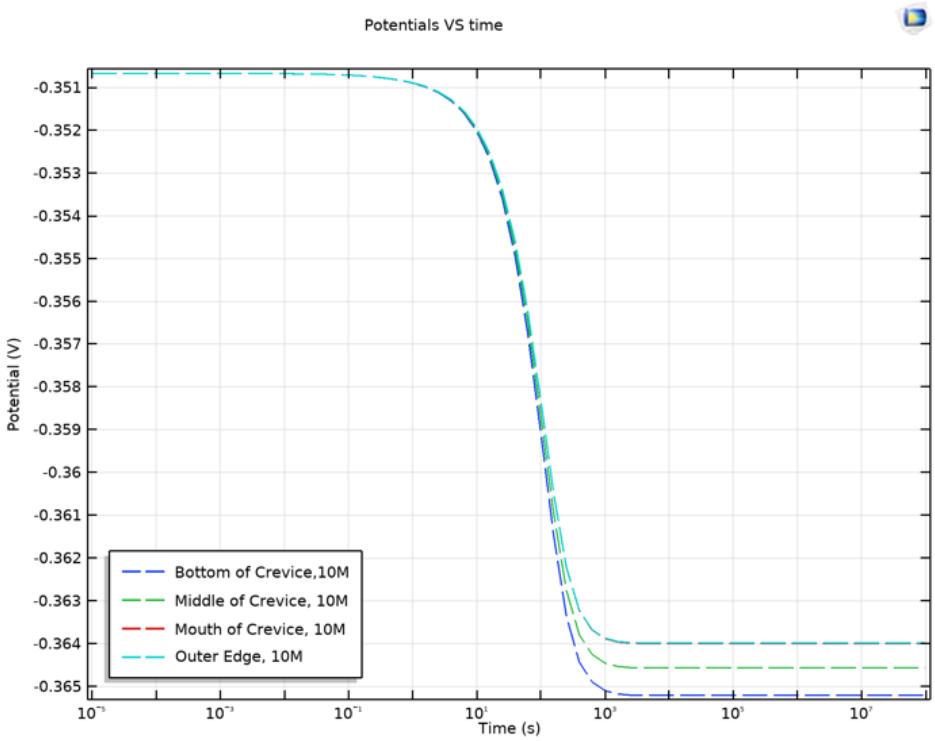

Fig. 4- 7: Simulation of potential as a function of time of iron in 10M NaCl solution. The result for 10M NaCl concentration represents by the dashed line. The blue dashed line represents the bottom of the crevice, the green dashed line represents the middle of the crevice, the red dashed line represents the mouth of the crevice and the cyan dashed line represents the outer edge.

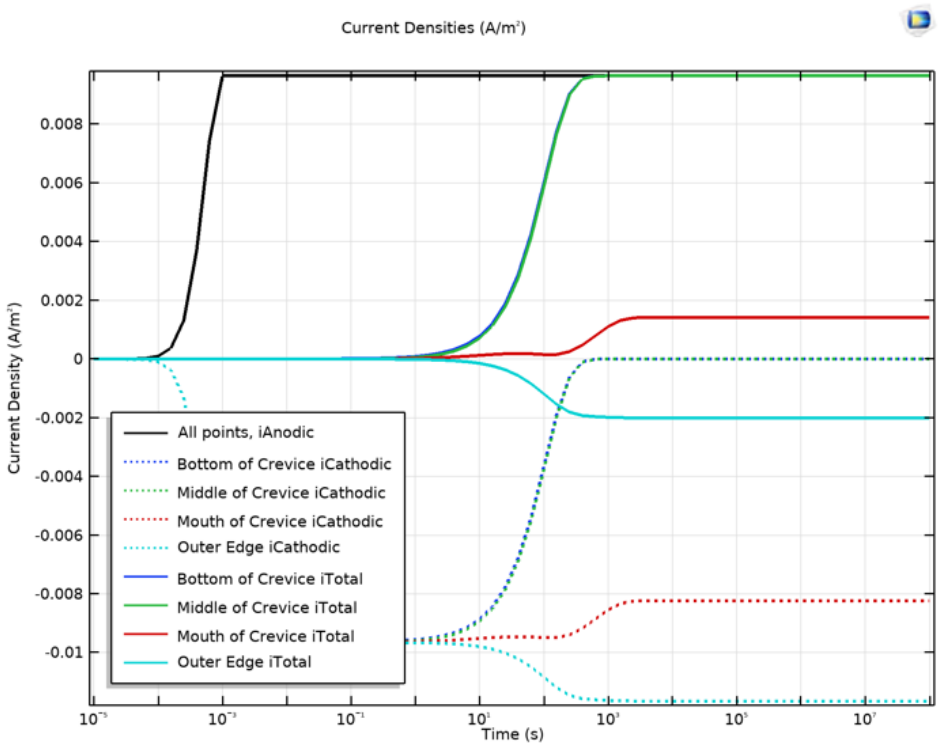

Fig. 4- 8: Simulation of current density with respect to time in 10M NaCl solution. Cathodic current represents by the dotted line with four colours representing four positions. Total current density represents by a solid line with four colours representing four points. Anodic current represents by one black solid line for all points, as it has the same profile for all positions.

Fig. 4-5 is a simulation of potential vs pH (Pourbaix diagram) in 10M NaCl solution. Potential at four positions (bottom of crevice, middle of crevice, mouth of crevice, and outer edge) were simulated and plotted with respect to pH. The 10M NaCl concentration in this study is governed by chloride ions. The result of 10M NaCl concentration represents by a dashed line and the four colours represent the positions in the geometry of nuts and bolts. A blue dashed line represents the bottom of the crevice, the green dashed line represents the middle of the crevice, a red dashed line represents the mouth of the crevice, and a cyan dashed line represents the outer edge. From the simulation in Fig.4-5, it shows that, no significant potential drop with respect to pH at all positions (outer edge, bottom, middle, and mouth of crevice).

Fig. 4-6 is a simulation of pH with respect to the time of iron nuts and bolts in 10M NaCl solution, where it is shown here that the pH increases at the beginning of the simulation, at all positions except at the outer edge and decreases in a later stage. At the initial time, pH outside of the crevice (mouth of crevice and outer edge) was set at 7 to ensure pH at the start

is in a neutral state. Meanwhile, pH inside the crevice (bottom and middle of crevice) was set slightly higher at 7.4 for better visualization but still within the neutrality region. Fig. 4-7 is the simulation of potential with respect to the time, of four positions of iron nuts and bolts in 10M NaCl concentration.

Initially, the pH of iron nut and bolt in 10M NaCl solution at all positions is neutral. As time passes by, pH at all positions starts to increase as shown in Fig. 4-6. This pH incremental can be explained by passive dissolution theory, where iron is undergoing a cathodic reaction forming iron ions (Fe^{2+}) and this cathodic reaction is balanced by an anodic reaction. The anodic reaction is the reaction where oxygen accepts electrons and produces hydroxide ions (OH^-). As anodic and cathodic reactions occurred on the iron metal, inside and outside of the crevice, more hydroxide ions in the solution caused the increase in pH value. In this thesis, the bottom and middle of the crevice are categorised as inside of the crevice. Meanwhile, the mouth of the crevice and outer edge is categorised as outside of the crevice. In 1.7 minutes, the pH inside of crevice (bottom and middle of crevice) increased from neutral pH of 7.4 to the peak pH of 10.4. Meanwhile, the pH at the mouth of the crevice increased from neutral pH of 7 to the peak of pH 9.5, at the same time (1.7 minutes). On the other hand, the pH at the outer edge increased from neutral pH of 7 to the peak of pH 9.1 in 3 minutes. From the simulation, it is shown that the inside of the crevice has the highest pH peak compared to the outside of the crevice.

As shown in Fig. 4-6, simulation of iron in 10M NaCl concentration, where pH starts to decrease with respect to time at the bottom, middle, and mouth of the crevice. The bottom and middle of the crevice enter the corrosion region in 5 minutes compared to the mouth of the crevice which enters the corrosion region in 33 minutes. Entering the corrosion region in this context means when the pH value is below pH 8.8 as shown in the Pourbaix diagram. As shown in the pourbaix diagram of iron in 10M NaCl solution (fig. 4-5), where the transition of iron metal from the passivity state (iron oxide Fe_3O_4) into the corrosion state (iron ions, Fe^{2+}). It is faster for the bottom and middle of the crevice to enter into the corrosion region, compared to the mouth of the crevice, because of the geometry. The bottom and middle of the crevice have a much narrower region and have a certain amount of oxygen initially present inside the crevice. This oxygen was used in the cathodic reaction to supplement the

iron anodic reaction. Because of the narrow nuts and bolts geometry, the oxygen diffusion rate into the crevice is much slower compared to the region outside the crevice. As time passes by, the amount of oxygen in the bottom and middle of the crevice starts to deplete and this is stated in the first stage of passive dissolution theory, which is oxygen depletion.

From the simulation in Fig. 4-6, it is shown that the pH at the bottom and middle of the crevice starts to decrease from the peak pH value of 10.4 at 1.7 minutes to the lowest pH of 6.1 for the bottom of the crevice and peak pH of 6.4 for the middle of the crevice, in 28 hours. Meanwhile, the pH at the mouth of the crevice decreased from a peak pH of 8.8 at 33 minutes to a pH of 7.8 in 28 hours. pH at the bottom, middle, and mouth of the crevice plateau after 28 hours at the pH value of 6.1, 6,4, and 7.8, respectively. A theoretical explanation for pH drop in the simulation in Fig. 4-6 is referring to the 2nd stage of passive dissolution theory, where essentially iron is undergoing a hydrolysis reaction, which produces both iron hydroxide and hydrochloric acid. Iron is undergoing an anodic reaction and continues producing iron ions (Fe^{2+}), which needs a counterbalance of the redox reaction which is a cathodic reaction. However, the narrow crevice geometry and oxygen depletion inside the crevice, cause the chloride (Cl^-) ions to diffuse into the crevice, in response to minimise the potential energy and balance the redox reaction. Iron ions react with chloride in the presence of aqueous, undergoing a hydrolysis reaction, forming metal hydroxides (FeOH) and hydrochloric acid (HCl). Presence of hydrochloric acid in the aqueous where the dissociation of Hydrogen ions (H^+) and chloride ions (Cl^-) is strong and thus a high amount of hydrogen ions (H+) present in the solution resulting in a low pH value. This theory complements the simulation, where the pH drops at the time of 1.7 minutes until 28 hours, for the bottom, middle, and mouth of the crevice.

In the simulation, the potential drops are parallel to pH drops within the time range of 1.7 minutes to 28 hours. At the time around 17 minutes, at the bottom and middle of the crevice, the potential drop from -351 mV to -365mV, gives a difference of 14 mV. At the mouth of the crevice and outer edge, a potential drop from -351 mV to -364 mV, gives a difference of 13 mV. pH at the bottom, middle, and mouth of the crevice reach a plateau after 28 hours of the pH value of 6.1, 6.4, and 7.8, respectively. However, pH at the outer edge reaches a plateau after 3 minutes at the peak pH value of 9.1. Other positions such as the bottom, middle, and

mouth of the crevice in the nuts and bolts geometry are restricted or semi-restricted with the oxygen diffusion, therefore the pH values at these 3 positions are low. This simulation validates that the region that has an abundance of oxygen, reduces the probability of oxygen depletion, acidification, and corrosion propagation. The convection rate used in this model is $2 \times 10\text{-}5\ m.s^{-1}$. Referring to passive dissolution theory, the third stage involves the crevice solution becoming more aggressive and destroying passive film and hydrogen ions, and chloride concentration will reach its maximum critical level. The fourth stage is that corrosion inside the crevice will propagate rapidly and the corrosion will become autocatalytic. It also stated that pH within the crevice could drop to pH 2.[34] In this simulation for 10M NaCl solution, the lowest pH achieved is pH 6.1. This simulation does not portray the last stage of passive dissolution theory perhaps due to the time allocated in the simulation itself, as it is not long enough to be able to monitor the later stages of passive dissolution theory.

Fig. 4-8 is a simulation of current density with time for a 10M NaCl ionic strength. Cathodic current represents by a dotted line with a blue dotted line representing the bottom of the crevice, a green dotted line represents the middle of the crevice, a red dotted line represents the mouth of the crevice and a cyan dotted line represents the outer edge. Anodic current represents by one black solid line at all positions, as all positions have a similar current density for anodic current. Total current density represents by a solid line with a blue solid line representing the bottom of the crevice, a green solid line representing the middle of the crevice, a red solid line representing the mouth of the crevice, and a cyan solid line representing an outer edge. This simulation shows the relationship between cathodic current density and anodic current density that results in total current density.

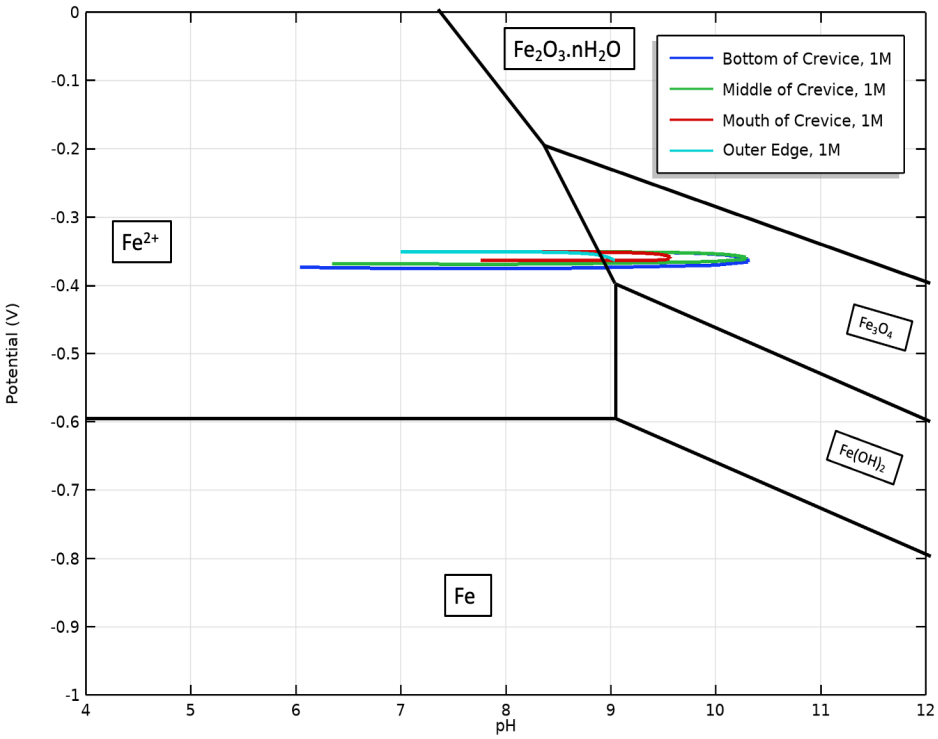

Fig. 4- 9: Pourbaix diagram of iron in 1M NaCl solution. The result for the 1M NaCl concentration study is represented by the solid line. The blue solid line represents the bottom of the crevice, the green solid line represents the middle of the crevice, the red solid line represents the mouth of the crevice and the cyan solid line represents the outer edge.

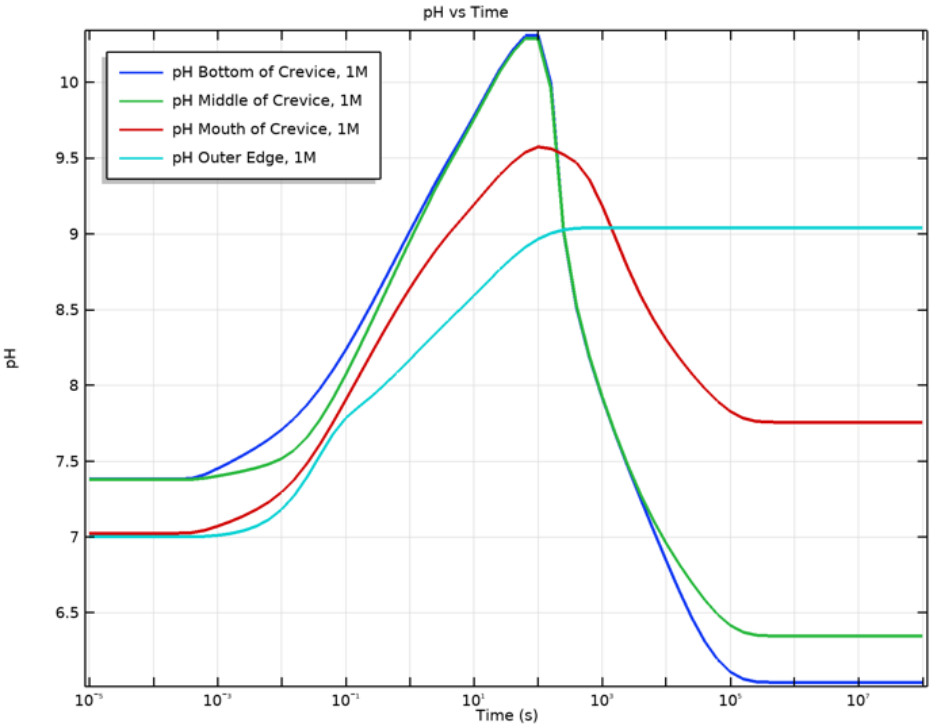

Fig. 4- 10: Simulation of pH as a function of time of iron in 1M NaCl solution. The result for the 1M NaCl concentration study is represented by the solid line. The blue solid line represents the bottom of the crevice, the green solid line represents the middle of the crevice, the red solid line represents the mouth of the crevice and the cyan solid line represents the outer edge.

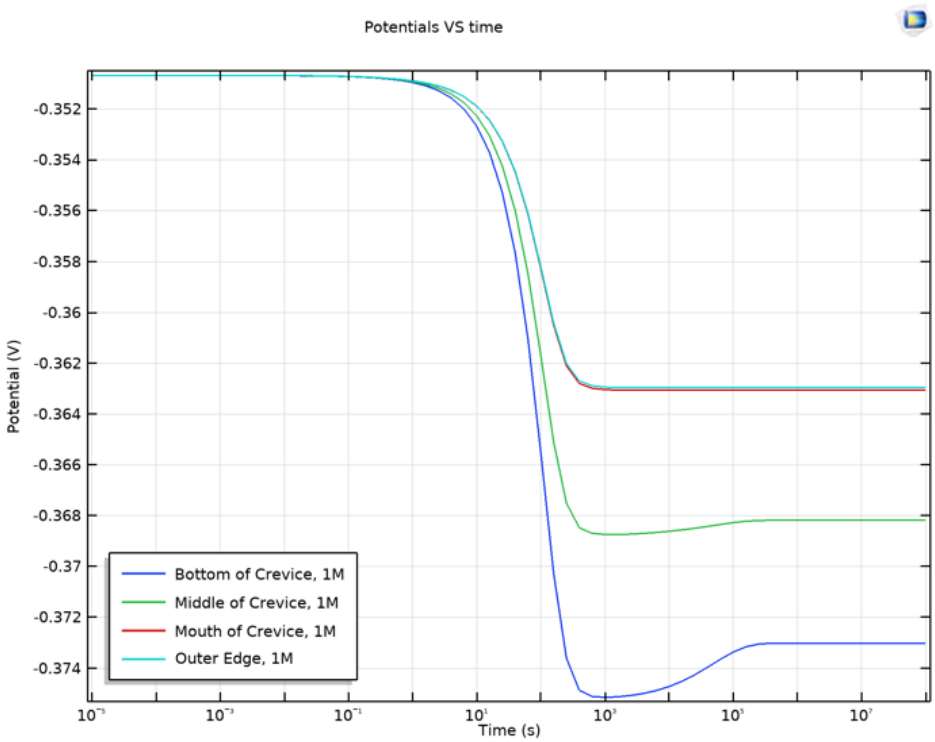

Fig. 4- 11: Simulation of potential as a function of time of iron in 1M NaCl solution. The result for the 1M NaCl concentration study is represented by the solid line. The blue solid line represents the bottom of the crevice, the green solid line represents the middle of the crevice, the red solid line represents the mouth of the crevice and the cyan solid line represents the outer edge.

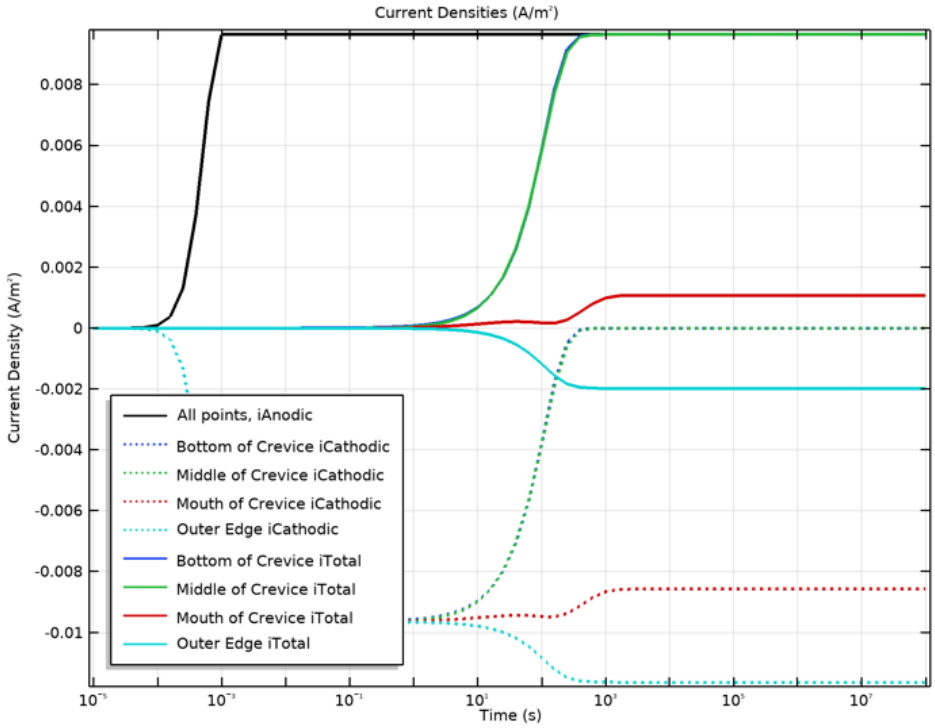

Fig. 4- 12: Simulation of current density with respect to time in 1M NaCl solution. Cathodic current represents by the dotted line with four colours representing four positions. Total current density represents by a solid line with four colours representing four points. Anodic current represents by one black solid line for all points, as it has the same profile for all positions

Fig. 4-9 is a simulation of potential vs pH in 1M NaCl solution, where the potential of 4 positions within the nuts and bolts geometry was simulated and plotted with respect to pH. The result of 1M NaCl concentration represents by solid lines and the four colours represent the positions in the geometry of nuts and bolts. A blue solid line represents the bottom of the crevice, a green solid line represents the middle of the crevice, a red solid line represents the mouth of the crevice, and a cyan solid line represents the outer edge.

Simulation of pH with respect to the time of iron in 1M NaCl solution is shown in Fig. 4-10. pH increases with respect to time in this simulation, at all positions except at the outer edge. At the initial time, the pH of iron nuts and bolts in 1M NaCl solution at all positions is neutral. With respect to time, an anodic reaction of iron metal is balanced by an oxygen reduction reaction which produced hydroxide ions (OH-). As more hydroxide ions were produced, the pH value increases. In less than 2 minutes, the pH at the bottom and middle of the crevice increases from pH of 7.4 to the peak value pH of 10.3. During the same time, the pH at the mouth of the crevice increases from neutral pH of 7 to the peak pH value of 9.6. Meanwhile, pH at the outer edge increases from neutral pH of 7 to the peak pH value of 9.1, in 3 minutes. pH begins to decrease with time at all positions except at the outer edge, as shown in fig. 4-10. pH at the bottom and middle of the crevice drops faster compared to the mouth of the crevice. The bottom and middle of the crevice entered the corrosion region in 3 minutes compared to the mouth of the crevice which entered the corrosion region in 33 minutes. The explanation for this phenomenon is due to the narrow region of crevice geometry. The mouth of the crevice is not fully limited by oxygen diffusion as in the bottom and middle of the crevice. Therefore the mouth of the crevice has more time before it reached oxygen depletion and acidification. Oxygen depletion is the 1st stage of passive dissolution theory.

In the bottom of the crevice, the pH drops from the time of 1.7 minutes to 28 hours, from the peak pH value of 10.3 to the lowest pH value of 6.1. In the middle of the crevice, pH drops from the peak value of pH 10.3 to the lowest pH value of 6.4, from 1.7 minutes to 28 hours. Meanwhile, the pH at the mouth of the crevice decrease from the peak pH value of 9.6 at 33 minutes to the pH value of 7.8 in 28 hours. pH at the bottom, middle, and mouth of the crevice plateau after 28 hours at the pH value of 6.1, 6,4, and 7.8, respectively. Scientific explanation during the pH drop as shown in the simulation in Fig. 4-10 is referring to the 2nd stage of

passive dissolution theory. In the 2nd stage of this theory, iron is undergone metal hydrolysis. Metal hydrolysis occurred when iron cations in the solution react with chloride ions in the water, forming metal hydroxides and hydrochloric acid. That leads to an increase of hydrogen ions presence in the solution resulting in a pH drop as shown in the simulation in Fig. 4-10, within the time range of 1.7 minutes to 28 hours.

Simulation of potential with respect to time in 1M NaCl solution is shown in Fig. 4-11. In the simulation, within the time range of 1.7 minutes to 28 hours, where the pH drops, the potential drops as well. At the time around 17 minutes, a potential drop from 351 mV to -374 mV for the bottom of the crevice, potential drops to -369 mV for the middle of the crevice, and potential drops to -363 mV for the mouth of the crevice and outer edge. For the outer edge and mouth of the crevice, the potential plateau remains at -363 mV. However in the middle and bottom of the crevice, the potential increases again before a plateau in 28 hours. For the bottom of the crevice, the potential increases from -374 mV to -373 mV. Meanwhile for the middle of the crevice, the potential increase from -369 mV to -368 mV. pH at all positions reaches a plateau after 28 hours, at different pH values depending on the position. The bottom, middle, and mouth of the crevice reach a plateau at the pH value of 6.1, 6.4, and 7.8 after 28 hours. Meanwhile, pH at the outer edge reaches a plateau after 3 minutes at the pH peak value of 9.1. A simulated pH probe that is placed outside of the crevice (at the outer edge position) does not experience pH drops due to the availability of oxygen and hence reduces the possibility and thermodynamics of corrosion.

The relationship between cathodic current density and anodic current density results in total current density is simulated and presented in Fig. 4-12. Fig. 4-12 is a simulation of current density with time for a 1M NaCl concentration study. Cathodic current represents by a dotted line with a blue dotted line representing the bottom of the crevice, the green dotted line represents the middle of the crevice, the red dotted line represents the mouth of the crevice and the cyan dotted line represents the outer edge. Anodic current density is represented by one black solid line for all points, as all points have the same current density for anodic current. Total current density represents by a solid coloured line with a blue solid line representing the bottom of the crevice, the green solid line representing the middle of the

crevice, the red solid line representing the mouth of the crevice, and the cyan solid line represents an outer edge.

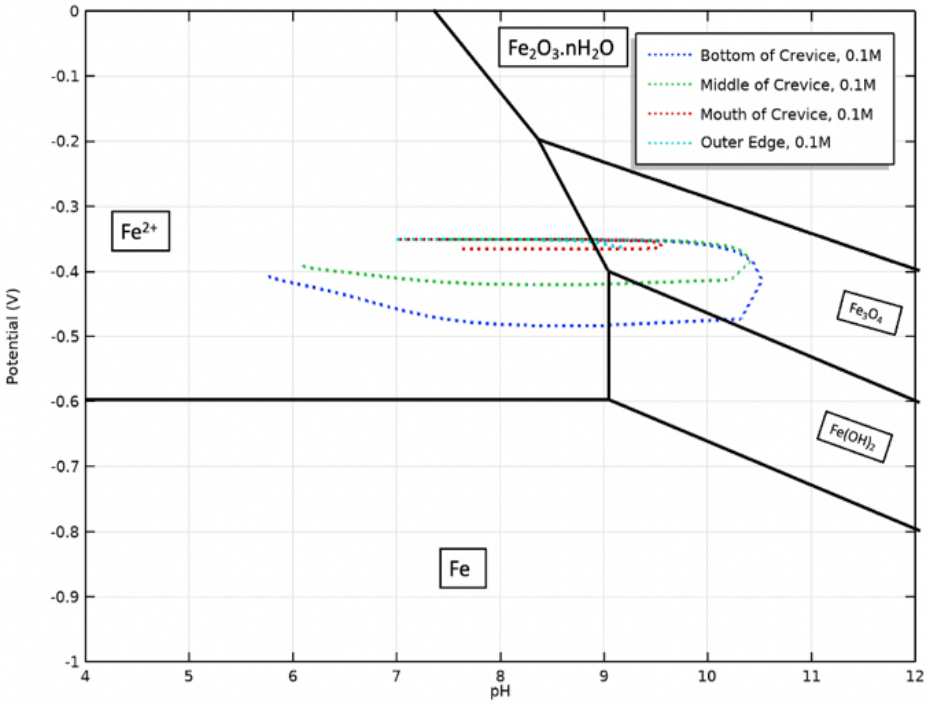

Fig. 4- 13: Pourbaix diagram of iron in 0.1M NaCl solution. The result for the 0.1M NaCl concentration study is represented by the dotted line. The blue dotted line represents the bottom of the crevice, the green dotted line represents the middle of the crevice, the red dotted line represents the mouth of the crevice and the cyan dotted line represents the outer edge.

Simulation of potential vs pH in 0.1M NaCl solution is shown in Fig. 4-13, in which four positions within the geometry of nuts and bolts were simulated and plotted with respect to pH. The result of 0.1M NaCl concentration represents by a dotted line and the four colours represent the positions in the geometry of nuts and bolts. The blue dotted line represents the bottom of the crevice, the green dotted line represents the middle of the crevice, a red dotted line represents the mouth of the crevice, and a cyan dotted line represents the outer edge.

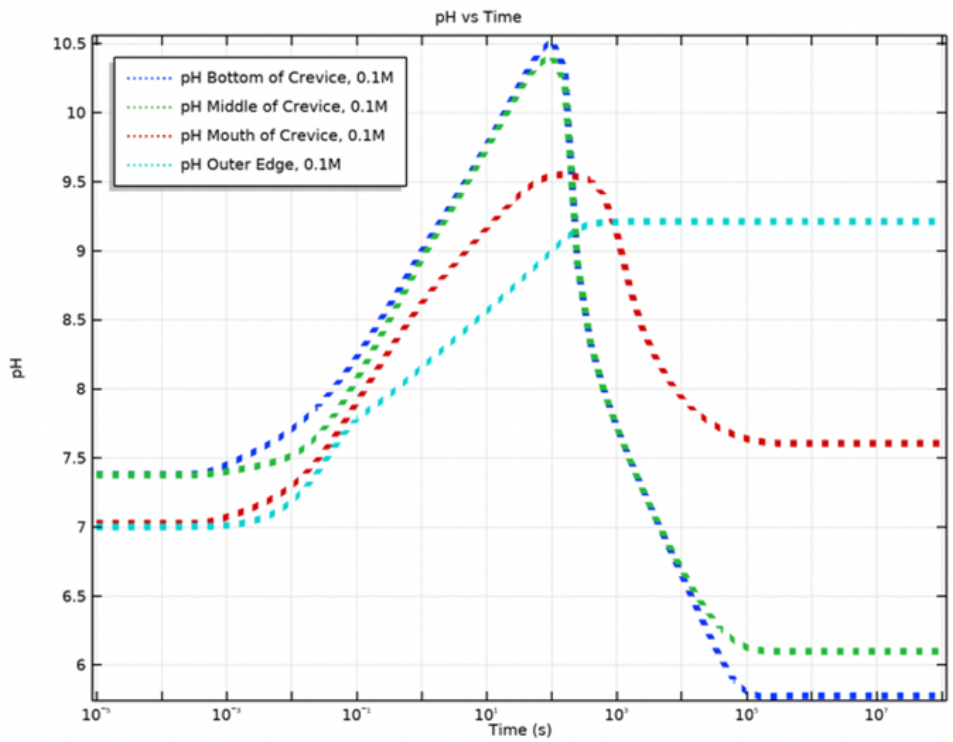

Fig. 4- 14: Simulation of pH as a function of time of iron in 0.1M NaCl solution. The result for the 0.1M NaCl concentration study is represented by the solid line. The blue dotted line represents the bottom of the crevice, the green dotted line represents the middle of the crevice, the red dotted line represents the mouth of the crevice and the cyan dotted line represents the outer edge.

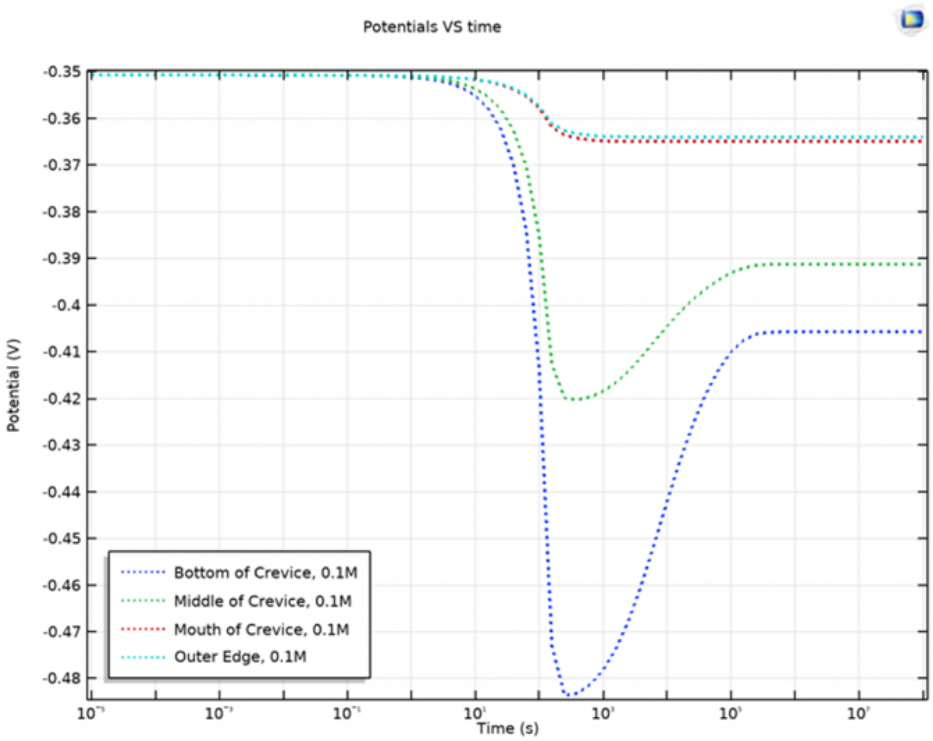

Fig. 4- 15: Simulation of potential as a function of time of iron in 0.1M NaCl solution. The result for the 0.1M NaCl concentration study is represented by the solid line. The blue dotted line represents the bottom of the crevice, the green dotted line represents the middle of the crevice, the red dotted line represents the mouth of the crevice and the cyan dotted line represents the outer edge.

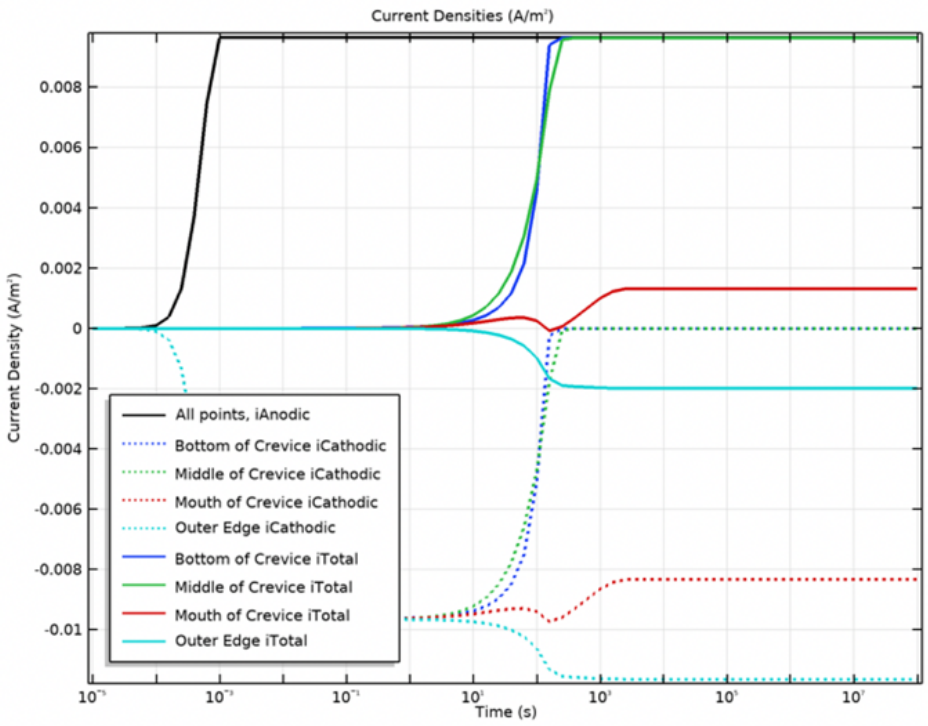

Fig. 4- 16: Simulation of current density with respect to time in 0.1M NaCl solution. Cathodic current represents by the dotted line with four colours representing four positions. Total current density represents by a solid line with four colours representing four points. Anodic current represents by one black solid line for all points, as it has the same profile for all positions

Fig. 4-14 is the simulation of pH with respect to the time of iron in 0.1M NaCl solution. pH increases as a function of time in this simulation, at all positions except the outer edge. At the initial time, the pH of nut and bolt in 0.1M NaCl solution at all positions is neutral. With respect to time, an anodic reaction of iron metal occurred and it is balanced by the cathodic reaction of oxygen reduction, that resulting in the formation of hydroxide ions. As the concentration of hydroxide ions in the solution increase, thus the pH values. In 1.7 minutes, the pH at the bottom and middle of the crevice increased from pH of 7.4 to the peak value pH of 10.5. On the other hand, the pH at the mouth of the crevice increased from neutral pH of 7 to the peak value pH of 9.5. Meanwhile, pH at the outer edge increased from neutral pH of 7 to the peak value pH of 9.1 in 3 minutes. pH begins to decrease with time for all positions except the outer edge, as shown in fig. 4-14. pH at the bottom and middle of the crevice, enter the corrosion region in 3 minutes compared to the pH at the mouth of the crevice which enters the corrosion region in 33 minutes. The mouth of the crevice is not fully limited by oxygen diffusion as in the bottom and middle of the crevice. Therefore bottom of the crevice

depletes its oxygen level much faster which leads to a higher rate of corrosion kinetics. Oxygen depletion is the 1st stage of passive dissolution theory.

The 2nd stage of passive dissolution theory is the metal hydrolysis which is represented by the pH drops in Fig. 4-14. From 1.7 minutes to 28 hours. At the bottom of the crevice, pH drops from its peak pH value of 10.5 to the lowest pH value of 5.8. In the middle of the crevice, pH drops from its peak pH value of 10.5 to the lowest pH value of 6.1. At the mouth of the crevice, pH drops from its peak pH value of 9.5 to the lowest pH value of 7.6. The scientific explanation behind this pH drop is that, the iron is undergoing metal hydrolysis, where iron cations react with chloride in aqueous, forming metal hydroxides and hydrochloric acid. The presence of hydrogen ions from the dissociation of hydrochloric acid in the water results in a pH drops, from 1.7 minutes to 28 hours.

Fig. 4-15 is a simulation of potential with respect to the time of iron nuts and bolts in 0.1M NaCl solution. In the simulation, potential drops within 17 minutes to 28 hours, meanwhile pH drops at 1.7 minutes to 28 hours as shown in Fig. 4-14. At the time around 17 minutes, at the bottom and middle of the crevice, the potential dropped from -351 mV to -480 mV and -420 mV, respectively. At the same time (17 minutes), at the mouth of the crevice and the outer edge, the potential dropped from -351 mV to -365 mV. The potential at the mouth of the crevice and at the outer edge does not increase and it remains at a plateau of -365 mV. Meanwhile, the potential at the bottom of the crevice increases from -480 mV to -405mV and remains plateau at -405 mV, after 28 hours. Potential at the middle of the crevice increase from -420 mV to -390 mV and remain plateau at -390 mV, after 28 hours. Referring to the pourbaix diagram in fig. 4-13 and simulation in fig. 4-15, the u-shaped potential profile indicates that there is a significant redox reaction of iron in 0.1M NaCl solution compared to 1M and 10M NaCl solution. In addition to that, from the simulation in Fig. 4-15, one can see that the bottom of the crevice has a much lower potential compared to the other positions in the nut and bolt geometry. This indicates that the bottom of the crevice has a higher redox reaction than other positions (mouth of crevice and outer edge). The bottom, middle, and mouth of the crevice reach a plateau at the pH value of 5.8, 6.1, and 7.6 after 28 hours. Meanwhile, pH at the outer edge reaches a plateau after 3 minutes at the peak value of 9.1. The pH probe that is placed outside of the crevice in the simulation (the outer edge) does not

record any pH drops due to the abundance of oxygen available and hence mitigates the anodic process.

Fig. 4.16 shows the relationship between cathodic current density and anodic current density that results in total current density. Fig. 4-16 is the simulation of current density with time for a 0.1M NaCl solution. Cathodic current represents by a dotted line with a blue dotted line representing the bottom of the crevice, the green dotted line represents the middle of the crevice, the red dotted line represents the mouth of the crevice, and the cyan dotted line represents the outer edge. Anodic current represents by one black solid line for all points, as all points have the same current density for anodic current. Total current density represents by a solid coloured line with a blue solid line representing the bottom of the crevice, a green solid line representing the middle of the crevice, a red solid line representing the mouth of the crevice, and a cyan solid line representing the outer edge.

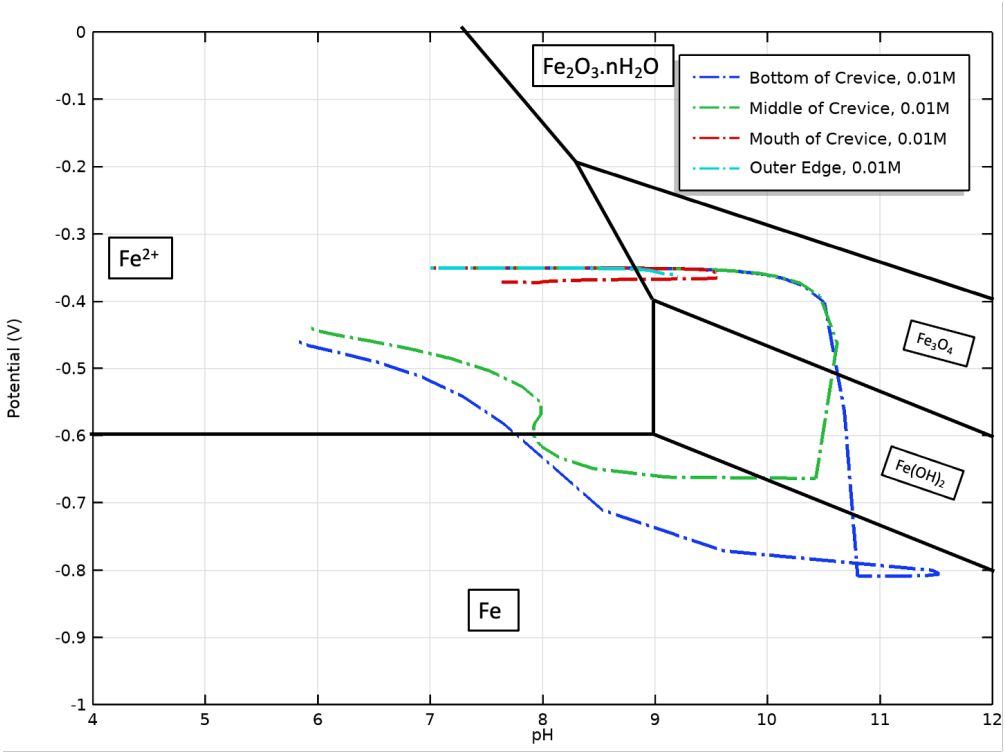

Fig. 4- 17: Pourbaix diagram of iron in 10M NaCl solution. The result for the 10M NaCl concentration study is represented by the dash-dotted line. The blue dash-dotted line represents the bottom of the crevice, the green dash-dotted line represents the middle of the crevice, the red dash-dotted line represents the mouth of the crevice and the cyan dash-dotted line represents the outer edge.

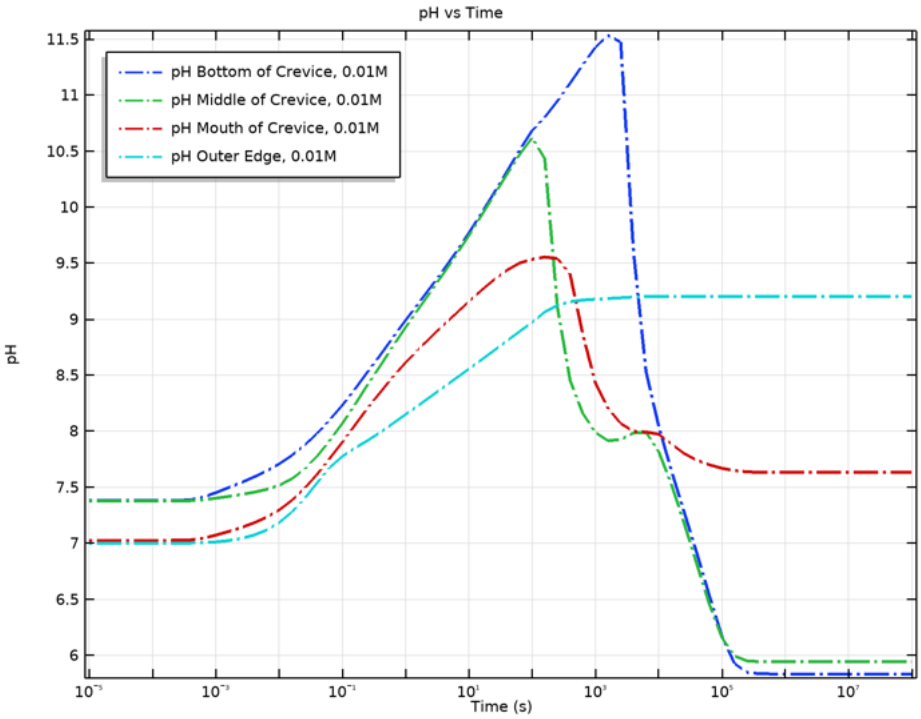

Fig. 4- 18: Simulation of pH as a function of time of iron in 0.01M NaCl solution. The result for the 0.1M NaCl concentration study is represented by the solid line. The blue dash-dotted line represents the bottom of the crevice, the green dash-dotted line represents the middle of the crevice, the red dash-dotted line represents the mouth of the crevice and the cyan dash-dotted line represents the outer edge.

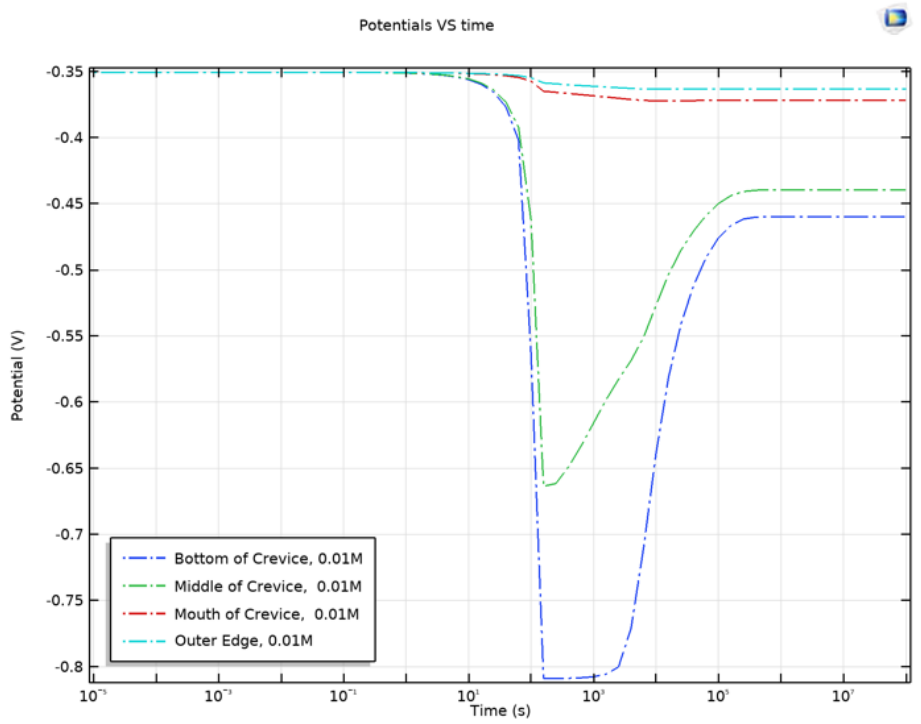

Fig. 4- 19: Simulation of potential as a function of time of iron in 0.01M NaCl solution. The result for the 0.1M NaCl concentration study is represented by the solid line. The blue dash-dotted line represents the bottom of the crevice, the green dash-dotted line represents the middle of the

crevice, the red dash-dotted line represents the mouth of the crevice and the cyan dash-dotted line represents the outer edge.

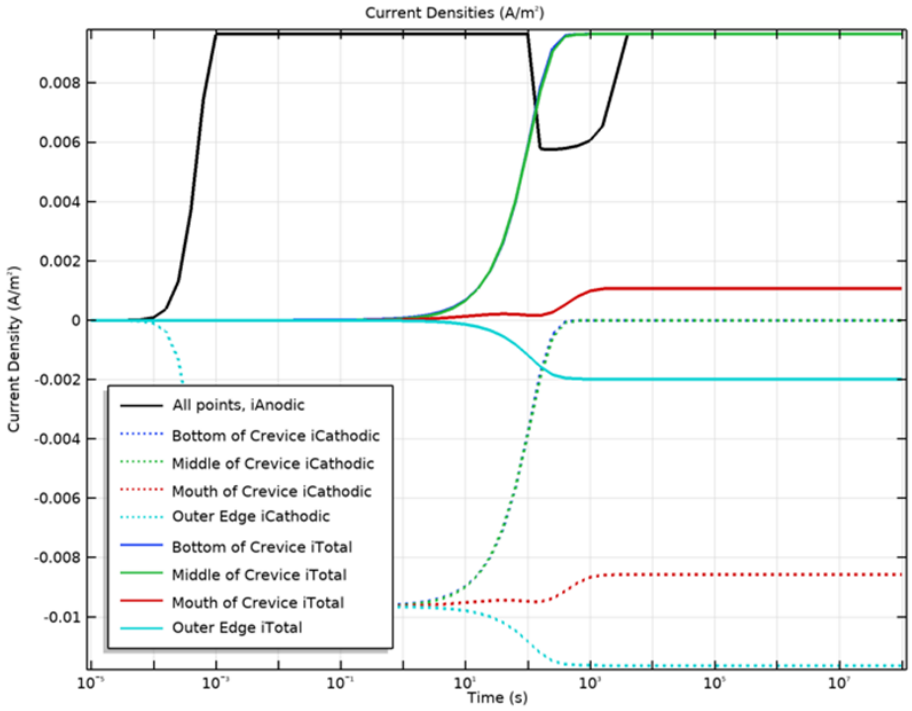

Fig. 4- 20: Simulation of current density with respect to time in 0.01M NaCl solution. Cathodic current represents by the dotted line with four colours representing four positions. Total current density represents by a solid line with four colours representing four points. Anodic current represents by one black solid line for all points, as it has the same profile for all positions

Fig. 4-17 is a simulation of potential vs pH (Pourbaix diagram) in 0.01M NaCl solution. Potential inside of crevice and outside or crevice were simulated and plotted with respect to pH. The result of 0.01M NaCl concentration represents by a dash-dotted line and the four colours represent the positions in the geometry of nuts and bolts. A blue dash-dotted line represents the bottom of the crevice, a green dash-dotted line represents the middle of the crevice, a red dash-dotted line represents the mouth of the crevice, and a cyan dash-dotted line represents the outer edge.

Fig. 4-18 is a simulation of pH with respect to the time of iron nuts and bolts in 0.01M NaCl solution, where it is shown that the pH increases at the beginning of the simulation, at all positions except the outer edge and decreases at the later stage. Initially, the pH of iron in 0.01M NaCl solution for all positions is neutral. With respect to time, pH at all positions starts to increase as shown in Fig. 4-18. This pH incremental can be explained by passive dissolution

theory, where iron is undergoing a cathodic reaction forming iron cations and balanced by an anodic reaction, that produces hydroxide ions. As anodic and cathodic reactions occurred inside and outside of the crevice, more hydroxide ions were present in the solution causing increases in pH value. From the simulation in Fig. 4-18, it took 20 minutes for the pH at the bottom of the crevice to reach its peak value of 11.5. Meanwhile, it took 1.7 minutes for the mouth and middle of the crevice to reach their peak pH values of 10.6 and 9.5, respectively. On the other hand, pH at the outer edge increased from neutral pH of 7 to the peak pH value of 9.1, in 3 minutes before the plateau. From the simulation, it is shown that the bottom of the crevice has the highest pH value peak compared to the other positions in the geometry. This finding shows that, in the lowest ionic strength (0.01M NaCl concentration), iron at the bottom of the crevice, has a higher cathodic reaction, which results in producing more hydroxide ions, that cause the solution becoming more alkaline.

As shown in Fig. 4-18, simulation of iron in 0.01M NaCl concentration, where pH starts to decrease with respect to time at the bottom, middle, and mouth of the crevice. The mouth and middle of the crevice enter the corrosion region in 10 minutes and 13 minutes, respectively. Meanwhile bottom of the crevice transition from the passivity region to the immunity region and it only enters the active corrosion region, as referred to the simulation in fig. 4-18 or the pourbaix diagram. It took 2.5 hours for the bottom of the crevice in 0.01M NaCl solution to enter into the corrosion region, compared to only 3 minutes in 1M NaCl solution for the same position (bottom of crevice). It took more time for a solution with lower ionic strength to enter the corrosion region due to its lower chloride concentration thus lower corrosion kinetic. As time passes by, oxygen concentration at the bottom, middle, and mouth of the crevice start to deplete and this is stated in the first stage of passive dissolution theory, which is oxygen depletion.

From the simulation in Fig. 4-18, it is shown that pH at the bottom of the crevice decreases from the peak pH value of 11.5 to pH 5.8 within 2.5 hours to 28 hours, where pH plateau at 5.8. In the middle of the crevice, pH decreases from a peak pH value of 10.6 to a pH of 5.9 in a time range of 1.7 minutes to 28 hours, where it plateaus at pH 7.6. At the mouth of the crevice, pH decreases from a pH peak value of 9.5 to a pH of 7.6 in the time range of 1.7 minutes to 28 hours, where pH plateaus at 7.6. At the outer edge, the pH increase from pH 7

to pH 9.2, and its plateaus. A theoretical explanation for pH drop in the simulation as shown in Fig. 4-18 is referring to the 2nd stage of passive dissolution theory, where iron is undergoing an iron hydrolysis reaction, which produces both iron hydroxide and hydrochloric acid. Hydrochloric acid in aqueous means a high concentration of hydrogen ions present in the solution resulting in a low pH value. This theory complements the simulation, where the pH drops at a time of approximately 1.7 minutes for the middle and mouth of the crevice and approximately 20 minutes for the bottom of the crevice.

In the simulation, within the timeframe where the pH drops (1.7 minutes to 28 hours) the potential decrease. Fig. 4-19 is the simulation of potential with respect to the time of iron nut and bolt in 0.01M NaCl concentration. At the time of around 1.7 minutes, potential drops from -351 mV to -790 mV at the bottom of the crevice, to -660 mV at the middle of the crevice, -370 mV at the mouth of the crevice, and -365 mV at the outer edge. Potential at the outer edge and mouth of crevice does not increase back and remains plateau at -365 mV and -370 mV. Meanwhile potential at the middle of the crevice increases from -660 mV to -440 mV in 28 hours, where it remains plateau after that. On the other hand, the potential at the bottom of the crevice increases from -790 mV to -460 mV, in 28 hours and remains plateau. Referring to the pourbaix diagram in fig. 4-17 and simulation in fig. 4-19, the decrease and increase in potential indicate that there is a significant redox reaction of iron in 0.01M NaCl solution compared to 1M and 10M NaCl solution. On top of that, from the simulation in Fig. 4-19, it is shown that the bottom of the crevice has a much lower potential compared to the same position (bottom of crevice) in others NaCl solutions; 10M, 1M and 0.1M NaCl solution. pH at the bottom, middle, and mouth of the crevice reaches a plateau at the pH value of 5.8, 5.9, and 7.6 after 28 hours. Meanwhile, pH at the outer edge reaches a plateau after 3 minutes at the peak value of 9.2. In the simulation, the pH probe that is placed outside of the crevice (outer edge) does not record any pH drop due to the abundance of oxygen available hence eliminating the acidification and metal dissolution.

Fig. 4-20 is the simulation of current density with time for a 0.01M NaCl conductivity study. Cathodic current represents by a dotted line with a blue dotted line representing the bottom of the crevice, a green dotted line represents the middle of the crevice, a red dotted line represents the mouth of the crevice and a cyan dotted line represents the outer edge. Anodic

current represents by one black solid line for all points, as all points have the same current density for anodic current. Total current density represents by a solid coloured line with a blue solid line representing the bottom of the crevice, a green solid line representing the middle of the crevice, a red solid line representing the mouth of the crevice, and a cyan solid line representing the outer edge. This simulation shows the relationship between cathodic current density and anodic current density that results in total current density.

4.2 Influence of crevice width

Key findings in the subchapter 4.1-Influence of solution ionic strength, are that oxygen depletion causes the acidification within the crevice and propagates the corrosion process. This subchapter 4.2 is presenting the simulation and findings on how crevice width is influencing the oxygen concentration within geometry and hence affecting the corrosion kinetics.

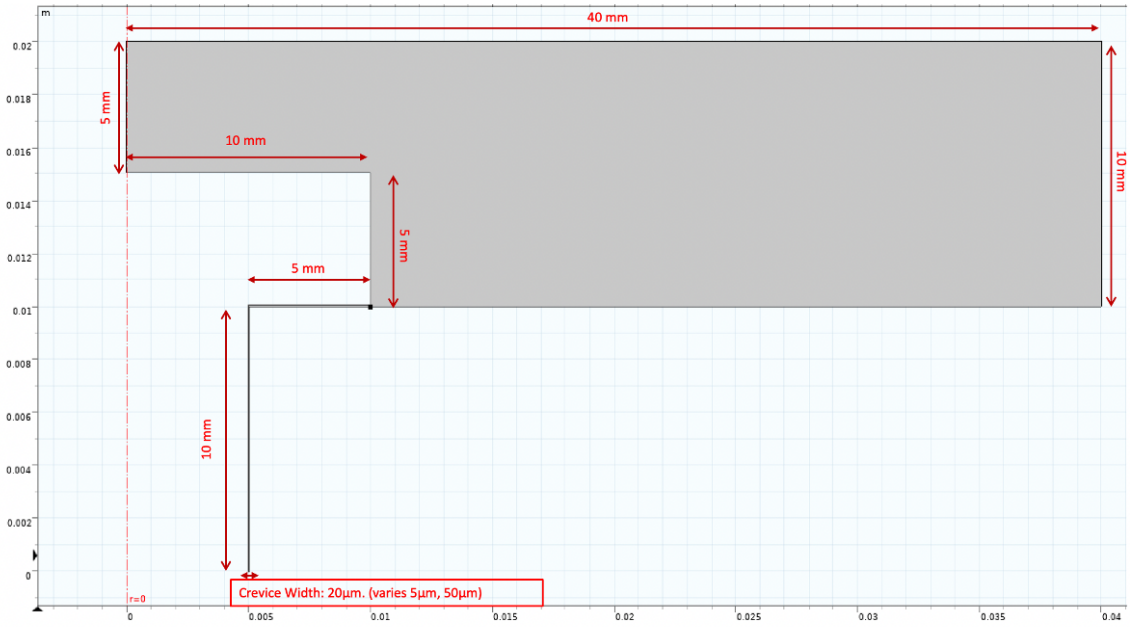

Fig. 4- 21: Dimension of Geometry 1, where the crevice depth is 10 mm. Width of crevice was varied at 5µm, 20µm or 50µm.

Fig. 4-21 is the dimension of iron nut and bolt with the depth of 10mm for geometry 1 in this thesis. Fig. 4-22 is the dimension of iron nuts and bolts with a depth of 20mm and this is known as geometry 2 in this thesis. Crevice widths were varied at 5 µm, 20 µm and 50 µm for geometry 1. Meanwhile, for geometry 2, crevice widths were varied at 5 µm, 10 µm, 20 µm and 50 µm. The main difference between geometry 1 and geometry 2 is the depth of the

crevice. The solution ionic strength of NaCl in this study was kept constant at 1M and initial concentration of oxygen is 0.25 mol.m^{-3}.

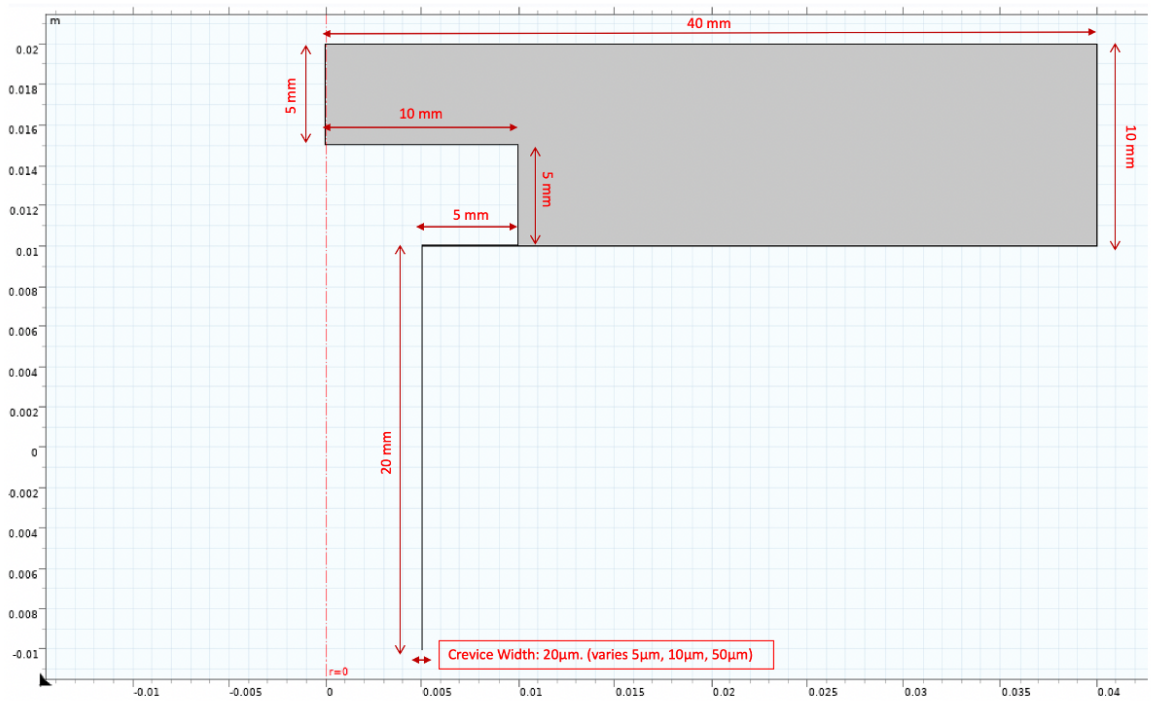

Fig. 4- 22: Dimension of Geometry 1, where the crevice depth is 10 mm. Width of crevice was varied at 5µm, 10µm, 20µm or 50µm.

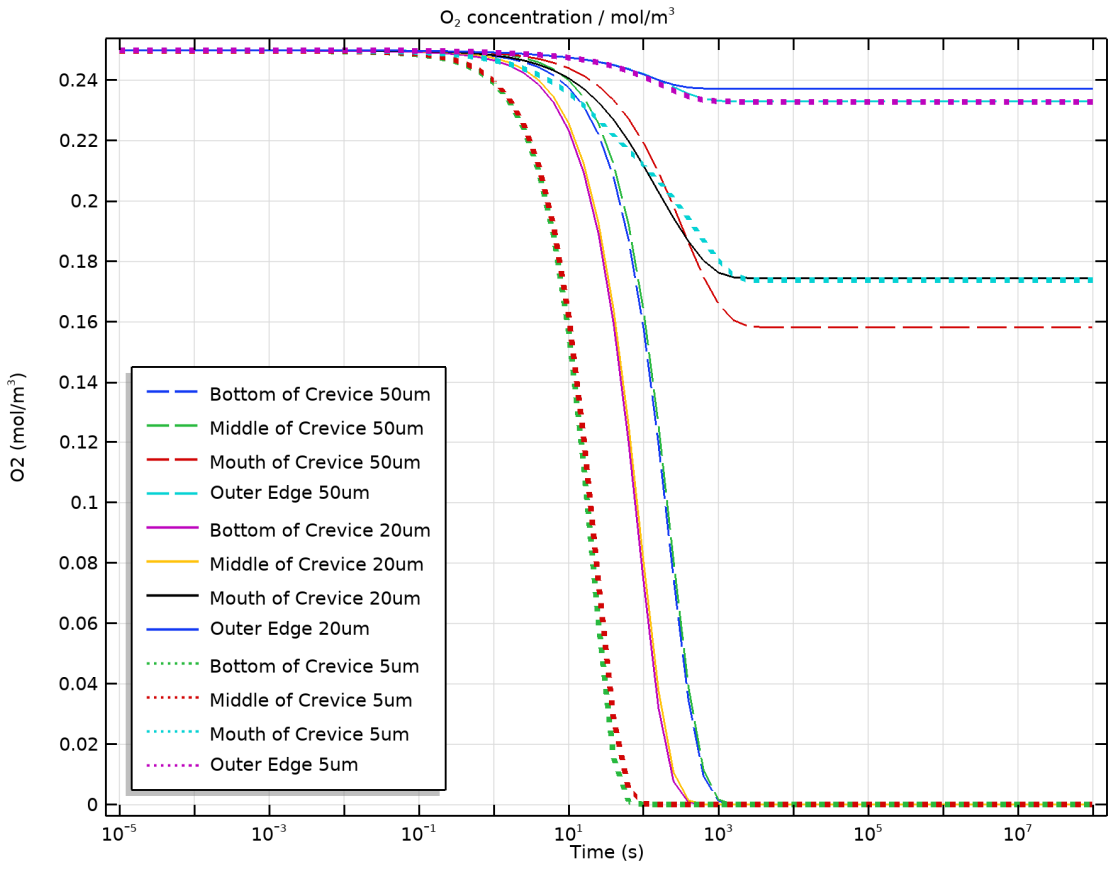

Fig. 4- 23: Simulation of oxygen concentration with respect to time of iron in 1M NaCl solution. The dashed lines represent the results of 50μm crevice width, the solid lines represent the results of 20 μm crevice width, and the dotted lines represent the result for 5μm crevice width.

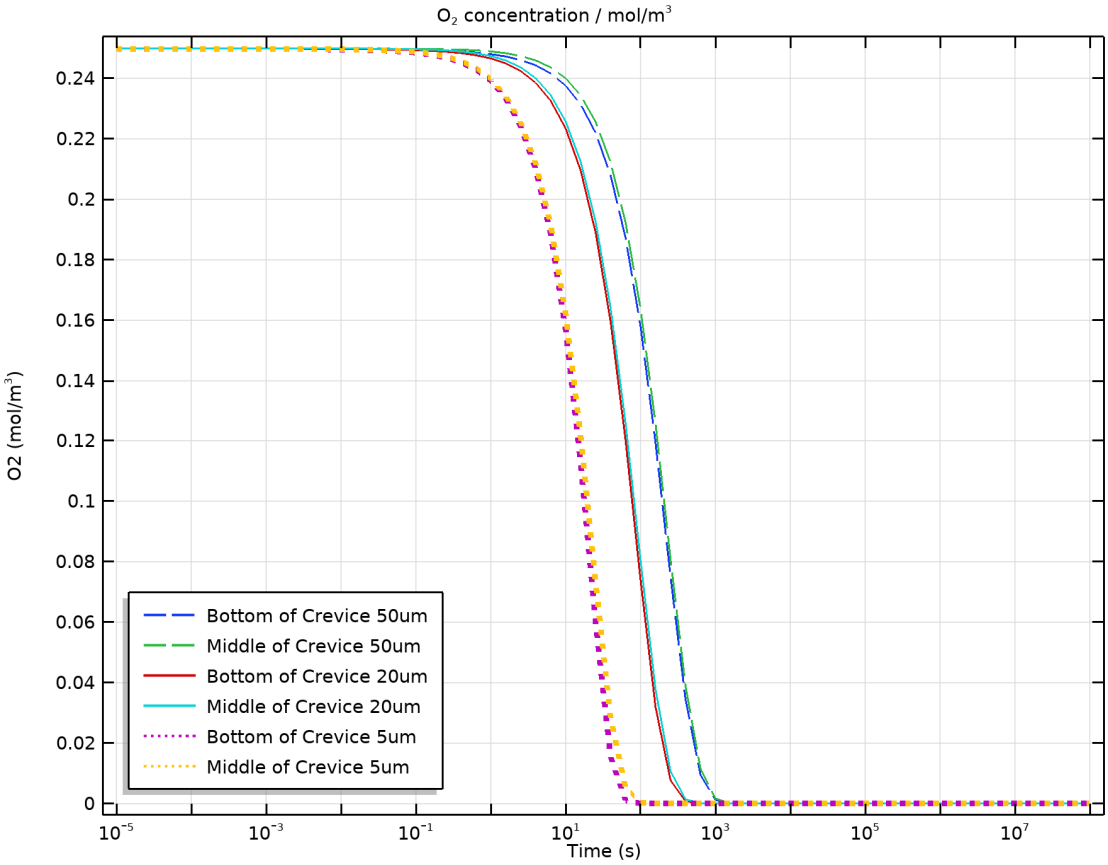

Fig. 4- 24: Simulation of oxygen concentration with respect to time of iron in 1M NaCl solution. The dashed blue and green lines represent the results of the bottom and middle of crevice at 50μm crevice width, the red and cyan solid lines represent the results of the bottom and middle of crevice at 20μm crevice width, and the purple and yellow dotted lines represent the result of the bottom and middle of crevice at 5μm crevice width.

Fig. 4-23 is a simulation of oxygen concentration with respect to time at geometry 1 at three different crevice widths; 5 μm, 20 μm, and 50 μm. A dashed line represents the result for 50 μm crevice width, a solid line represents the result for 20 μm crevice width, a dotted line represents a result for 5 μm crevice width. The cyan dashed line represents the outer edge of 50 μm crevice width, the blue solid line represents the outer edge of 20 μm crevice width, the purple dotted line represents the outer edge of 5 μm crevice width. From the simulation in Fig. 4-23, at the outer edge, oxygen decreased from its initial concentration of 0.25 mol.m^{-3} to approximately 0.23 mol.m^{-3} after 17 minutes. Oxygen at the outer edge does not deplete

completely due to the availability of oxygen outside the crevice, where the convection rate introduced in this simulation is 2x10-5 $m.s^{-1}$.

From the simulation in fig. 4-23, the red dashed line represents the mouth of the crevice of 50 μm crevice width, the black solid line represents the mouth of the crevice of 20 μm crevice width, the cyan dotted line represents the mouth of the crevice of 5 μm crevice width. Oxygen at the mouth of the crevice does not deplete completely as the position of the mouth of the crevice is partially exposed to the outer environment. At the mouth of the crevice, where the initial oxygen concentration is 0.25 $mol.m^{-3}$ and the oxygen concentration decrease to 0.16 $mol.m^{-3}$ after 27 minutes for 50 μm crevice width. Meanwhile for both; 20 μm and 5 μm crevice width, the oxygen concentration decreased to 0.175 $mol.m^{-3}$ after 27 minutes.

Fig. 4-24 is the magnified plot of the simulation in fig. 4-23 that focus on the bottom and middle of the crevice. From the findings in fig. 4-24, the green dashed line represents the middle of the crevice of 50 μm crevice width, the cyan solid line represents the middle of the crevice of 20 μm crevice width, the yellow dotted line represents the middle of the crevice of 5 μm crevice width. The blue dashed line represents the bottom of the crevice of 50 μm crevice width, the red solid line represents the bottom of the crevice of 20 μm crevice width, the purple dotted line represents the bottom of the crevice of 5 μm crevice width. As shown in the simulation in Fig. 4-24, oxygen in the middle and bottom of the crevice depletes its oxygen completely from 0.25 $mol.m^{-3}$ to 0 $mol.m^{-3}$, and both positions; the middle and bottom of the crevice deplete its oxygen content relatively at the same time.

For 50 μm crevice width, the oxygen concentration at the bottom and middle of the crevice depletes completely within 21 minutes. Meanwhile, for 20 μm crevice width, the oxygen concentration at the bottom and middle of the crevice depletes completely within 8 minutes. Lastly, for 5 μm crevice width, the oxygen concentration at the bottom and middle of the crevice depletes completely in less than 2 minutes. Oxygen concentration in the smallest crevice width (5 μm) is depleting much faster compared to bigger crevice width (20 μm, 50 μm) crevice widths because the smallest crevice width has a low initial amount of oxygen present inside the crevice. In addition, due to the narrower region of 5 μm crevice width, it is

much more challenging for oxygen to diffuse into the 5 μm crevice width compared to 50 μm crevice width. This results in a lower oxygen diffusion rate into the crevice width that causes oxygen depletion inside the crevice. Summary and comparison of the time taken for oxygen to decrease its initial oxygen concentration of 0.25 mol.m^{-3} is tabulated in table 4.1.

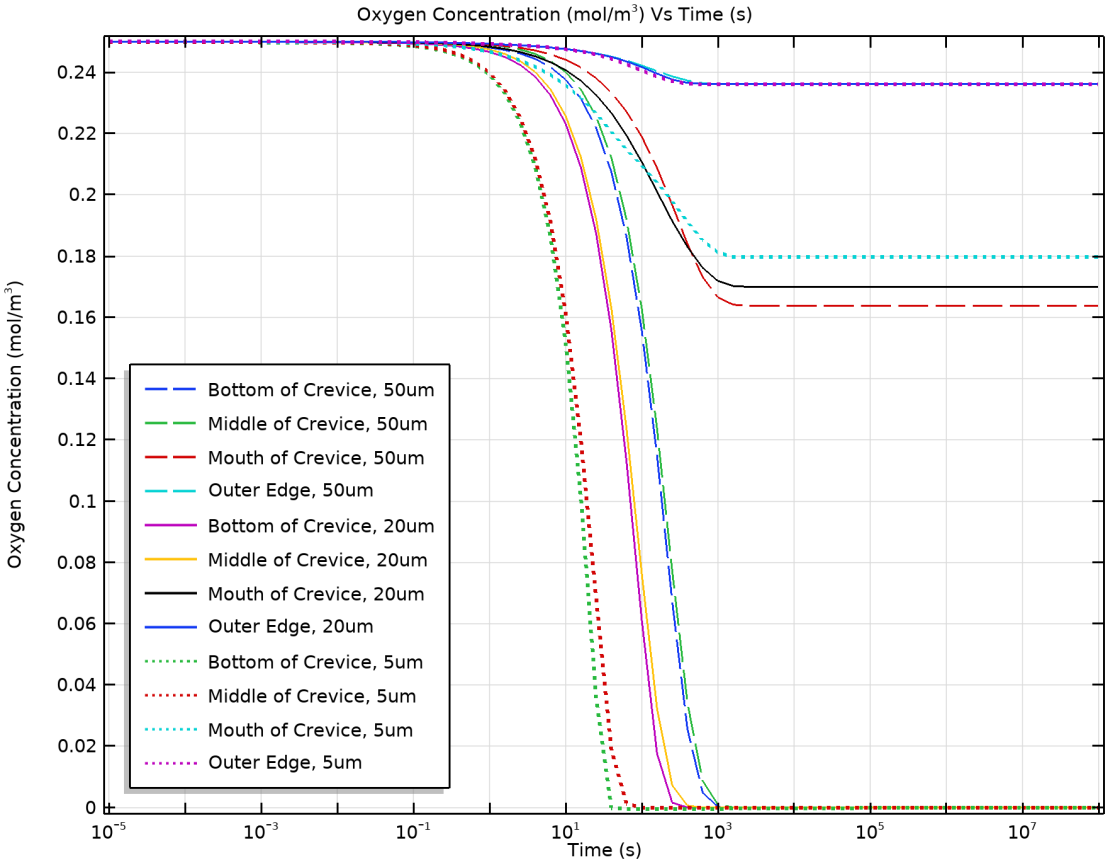

Fig. 4- 25: Simulation of oxygen concentration with respect to time of iron in 1M NaCl solution. The dashed lines represent the results of 50μm crevice width, the solid lines represent the results of 20μm crevice width, and the dotted lines represent the result for 5μm crevice width.

Fig. 4-25 is a simulation of oxygen concentration with respect to time at geometry 2 at crevice widths of 5 μm, 20 μm, and 50 μm. A dashed line represents the result for 50 μm crevice width, a solid line represents the result for 20 μm crevice width, a dotted line represents the result for 5 μm crevice width. The cyan dashed line represents the outer edge of 50 μm crevice width, the blue solid line represents the outer edge of 20 μm crevice width, and the purple dotted line represents the outer edge of 5 μm crevice width. From the simulation in Fig. 4-25, at the outer edge, oxygen decreases from its initial concentration of 0.25 mol.m^{-3} to

approximately 0.23 mol.m^{-3} after 7 minutes. Oxygen at the outer edge does not deplete completely due to the availability of oxygen outside the crevice.

Referring to the simulation in fig. 4-25, a red dashed line represents the mouth of the crevice of 50 μm crevice width, a black solid line represents the mouth of the crevice of 20 μm crevice width, cyan dotted line represents the mouth of the crevice of 5 μm crevice width. Oxygen at the mouth of the crevice does not deplete completely as the position is exposed to the environment partially. The initial oxygen concentration is 0.25 mol.m^{-3} and it decreases to 0.165 mol.m^{-3} after 27 minutes for 50 μm crevice width, at the mouth of the crevice. Meanwhile, for both; 20 μm and 5 μm crevice width, the oxygen concentration decreased to 0.17 mol.m^{-3} and 0.18 mol.m^{-3} after 27 minutes.

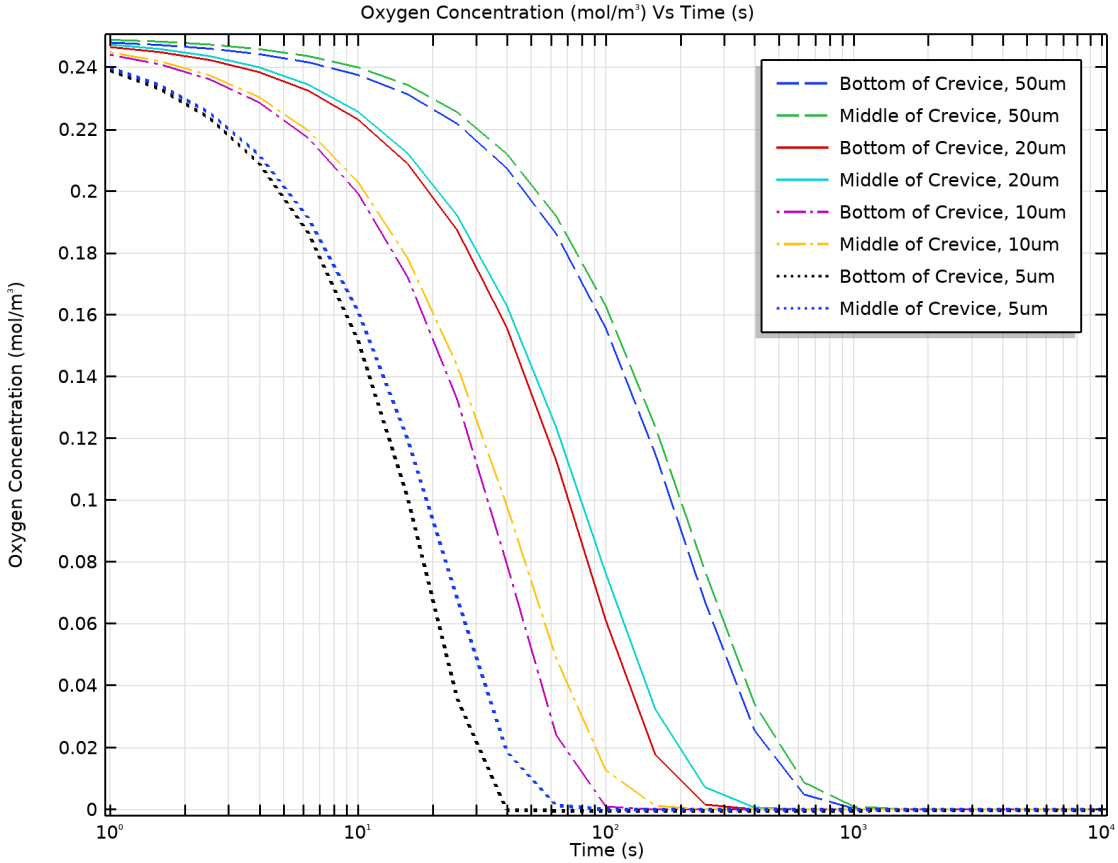

Fig. 4- 26: Simulation of oxygen concentration with respect to time of iron in 1M NaCl solution. The dashed blue and green lines represent the results of the bottom and middle of crevice at 50μm crevice width, the red and cyan solid lines represent the results of the bottom and middle of crevice at 20μm crevice width, and the purple and yellow dash-dotted lines represent the result of the bottom and middle of crevice at 10μm crevice width. The dotted lines represent the result of the bottom and middle of crevice at 5μm crevice width.

An enlarged graph of the simulation in fig 4-25 is represented in fig. 4-26, that is focusing on the bottom and middle of the crevice. In addition, 10 μm crevice width was simulated and shown in fig. 4-26. From the findings in fig. 4-26, green dashed line represents the middle of the crevice of 50 μm crevice width, a cyan solid line represents the middle of the crevice of 20 μm crevice width, a blue dotted line represents the middle of the crevice of 5 μm crevice width, a yellow dash-dotted line represents the middle of the crevice of 10 μm crevice width.

For the bottom of the crevice, the blue dashed line represents the bottom of the crevice of 50 μm crevice width, the red solid line represents the bottom of the crevice of 20 μm crevice width, black dotted line represents the bottom of the crevice of 5 μm crevice width, the purple dash-dotted line represents the bottom of the crevice of 10 μm crevice width. As shown in the simulation in Fig. 4-26, oxygen in the middle and bottom of the crevice depletes its oxygen completely to 0 $mol.m^{-3}$, at a relatively the same time. For 50 μm crevice width, the oxygen concentration at the bottom and middle of the crevice deplete completely within 17 minutes. Meanwhile, for 20 μm crevice width, the oxygen concentration at the bottom and middle of the crevice deplete completely within 4 minutes. Meanwhile, for 10 μm crevice width, the oxygen concentration depletes completely within 3 minutes. For 5 μm crevice width, the oxygen concentration at the bottom and middle of the crevice deplete completely in 25 seconds and 80 seconds.

The biggest the crevice width, the more time is needed to deplete the oxygen concentration. 50 μm crevice width needed 17 minutes to deplete its oxygen concentration compared to 0.42 minutes for 5 μm crevice width. Apart from that, smaller crevice width has a narrower region, which makes it difficult for oxygen to diffuse into the crevice width of 5 μm compared to of crevice width of 50 μm. This results in a lower oxygen diffusion rate into the crevice width that causes oxygen depletion inside the crevice. Summary and comparison of the time

taken for oxygen to decrease oxygen concentration from 0.25 mol.m^{-3} in geometry 2 is tabulated in table 4-2.

Another key finding in this research, comparing the 2 summarised tables which are table 4-1 and table 4-2. It is shown here that the time taken for oxygen to deplete inside the crevice, in geometry 2 is much faster compared to geometry 1, despite the geometry 2 has double the depth of geometry 1 (geometry 2 has a depth of 20 mm and geometry 1 has the depth of 10mm). From this simulation, it is shown that deeper crevice depth has a higher oxygen depletion rate that leads to higher kinetic of crevice corrosion.

Table 4- 1: Time is taken for oxygen to decrease from 0.25 mol.m^{-3} to 0 mol.m^{-3} at the bottom and middle of crevice with 5 μm, 20 μm, 50 μm crevice width in Geometry 1. Time is taken to for oxygen to decrease from 0.25 mol.m^{-3} to reach plateau value for outer edge and middle of crevice with 5 μm, 20 μm, and 50 μm crevice width in Geometry 1. The upper value in mol.m^{-3} is the value for oxygen concentration. The lower value in bracket () is the time taken the upper value for oxygen to reach.

Crevice Width	5 μm	20 μm	50 μm
Bottom of crevice	0 mol.m^{-3} (1.7 mins)	0 mol.m^{-3} (8 mins)	0 mol.m^{-3} (21 mins)
Middle of crevice	0 mol.m^{-3} (1.7 mins)	0 mol.m^{-3} (8 mins)	0 mol.m^{-3} (21 mins)
Mouth of crevice	0.175 mol.m^{-3} (27 mins)	0.175 mol.m^{-3} (27 mins)	0.16 mol.m^{-3} (27 mins)
Outer Edge	0.23 mol.m^{-3} (17 mins)	0.235 mol.m^{-3} (17 mins)	0.23 mol.m^{-3} (17 mins)

Table 4- 2: Time is taken for oxygen to decrease from 0.25 mol.m^{-3} to 0 mol.m^{-3} at the bottom and middle of crevice with 5 μm, 10 μm, 20 μm, and 50 μm crevice width in Geometry 2. Time is taken to for oxygen to decrease from 0.25 mol.m^{-3} to reach plateau value for outer edge and middle of crevice with 5 μm, 10 μm, 20 μm, 50 μm crevice width in Geometry 2. The upper value in mol.m^{-3} is the value for oxygen concentration. The lower value in bracket () is the time taken for oxygen to reach the upper value.

Crevice Width	5 μm	10 μm	20 μm	50 μm
Bottom of crevice	0 mol.m^{-3} (25 secs)	0 mol.m^{-3} (3 mins)	0 mol.m^{-3} (4 mins)	0 mol.m^{-3} (17 mins)
Middle of crevice	0 mol.m^{-3} (80 secs)	0 mol.m^{-3} (3 mins)	0 mol.m^{-3} (4 mins)	0 mol.m^{-3} (17 mins)
Mouth of crevice	0.18 mol.m^{-3} (27 mins)	n/a	0.17 mol.m^{-3} (27 mins)	0.165 mol.m^{-3} (27 mins)
Outer Edge	0.235 mol.m^{-3} (7 mins)	n/a	0.235 mol.m^{-3} (7 mins)	0.235 mol.m^{-3} (7 mins)

5.0 Conclusion & recommendation

The aim of this research is to investigate the crevice corrosion kinetics in iron nuts and bolts has achieved. A key finding from this research is that the simulation results were supported by passive dissolution theory. The simulation results showed that the pH of all NaCl solutions at all positions was increased initially due to the cathodic reaction (OH- production) that act as a counterbalance of metal dissolution. The result showed that oxygen inside the crevice depleted in minutes and this oxygen depletion is the first stage of the theory. Another key finding as shown in the second part of the simulation is the relationship between crevice width-depth and the oxygen concentration. The simulation result shows that oxygen inside the smallest and deepest crevice depleted faster due to the less initial oxygen presence and geometrical difficulty for oxygen to diffused-in. In the second stage of passive dissolution theory, as the anodic reaction continues, chloride ions diffused into the crevice and metal hydrolysis was observed, producing hydrogen ions, which resulted in the decrease of pH as shown in the simulation result. Based on the passive dissolution theory, the later stages, where crevice solution is more aggressive and destroys the passive film and propagates the corrosion process. However, the later stages were not observed in the simulation and thus, future research work is needed to extend the time of the simulation and observe and record the result.

Reference

1. Fontana, M. G. (Mars G. & Greene, N. D. *Corrosion Engineering*. (Mc-Graw Hil, 1967).

2. Koch, G. *et al.* International Measures of Prevention, Application, and Economics of Corrosion Technologies Study. *NACE Int.* 1–3 (2016).

3. ASTM G48-11. Standard test methods for pitting and crevice corrosion resistance of stainless steels and related alloys by use of ferric Chloride solution. *ASTM Int.* **03,** 1–10 (2003).

4. Revie, R. W., Uhlig, H. H. & Electrochemical Society. *Uhlig's corrosion handbook*. *The Electrochemical Society series* (2000). doi:10.1002/9780470872864.ch49

5. Pourbaix, M. *Atlas of electrochemical equilibria in aqueous solutions*. (Oxford etc. : Pergamon ; Brussels : Cebelcor, 1966).

6. Gaudet, G. T. *et al.* Mass transfer and electrochemical kinetic interactions in localized pitting corrosion. *AIChE J.* **32,** 949–958 (1986).

7. Evans, U. R. & Davies, D. E. The Pitting of Zinc by Distilled Water and Dilute Solutions. *J. Chem. Soc.* (1951). doi:10.1039/JR9510002607

8. Schafer, G. J., Gabriel, J. R. & Foster, P. K. On the Role of the Oxygen Concentration Cell in Crevice Corrosion and Pitting. *J. Electrochem. Soc.* **107,** 1002 (1960).

9. Schafer, G. J. & Foster, P. K. The Role of the Metal-Ion Concentration Cell in Crevice Corrosion. *J. Electrochem. Soc.* **106,** 468 (1959).

10. Evans, U. R. Metallic Corrosion, Passivity and Protection. *Arnold Co* 232 (1937). doi:10.1002/jctb.5000562112

11. Hoar, T. P., Mears, D. C. & Rothwell, G. P. The relationships between anodic passivity, brightening and pitting. *Corros. Sci.* **5,** 279–289 (1965).

12. Leckie, H. P. & Uhlig, H. H. Environmental Factors Affecting the Critical Potential for

Pitting in 18–8 Stainless Steel. *J. Electrochem. Soc.* **113,** 1262 (1966).

13. Böhni, H. & Uhlig, H. H. Environmental Factors Affecting the Critical Pitting Potential of Aluminum. *J. Electrochem. Soc.* **116,** 906 (1969).

14. Oldfield, J. W. & Sutton, W. H. Crevice Corrosion of Stainless Steels: I. A Mathematical Model. *Br. Corros. J.* **13,** 13–22 (1978).

15. Lott, S. E. & Alkire, R. C. The variation of solution composition during the initiation of crevice corrosion on stainless steel. *Corros. Sci.* **28,** 479–484 (1988).

16. Nash, B. K. & Kelly, R. G. Characterization of the crevice solution chemistry of 304 stainless steel. *Corros. Sci.* **35,** 817–825 (1993).

17. Sridhar, N. & Dunn, D. S. Effect of applied potential on changes in solution chemistry inside crevices on type 304L stainless steel and alloy 825. *Corrosion* **50,** 857–872 (1994).

18. Laycock, N. J., Stewart, J. & Newman, R. C. THE INITIATION OF CREVICE CORROSION STEELS IN STAINLESS. *Corros. Sci.* **39,** 1791–1809 (1997).

19. Kennell, G. F., Evitts, R. W. & Heppner, K. L. A critical crevice solution and IR drop crevice corrosion model. *Corros. Sci.* **50,** 1716–1725 (2008).

20. Pickering, H. W. & Frankenthal, R. P. On the Mechanism of Localized Corrosion of Iron and Stainless Steel. *J. Electrochem. Soc.* **119,** 1297–1304 (1972).

21. Lott, S. E. & Alkire, R. C. The Role of Inclusions on Initiation of Crevice Corrosion of Stainless Steel: I . Experimental Studies. *J. Electrochem. Soc.* **136,** 973–979 (1989).

22. Alkire, R. C. & Lott, S. E. The Role of Inclusions on Initiation of Crevice Corrosion of Stainless Steel II . Theoretical Studies. *J. Electrochem. Soc.* **136,** 3256–3262 (1989).

23. Stockert, L. & Böhni, H. Susceptibility to Crevice Corrosion and Metastable Pitting of Stainless Steels. *Mater. Sci. Forum* **44–45,** 313–328 (1989).

24. Suleiman, M. I., Ragault, I. & Newman, R. C. The pitting of stainless steel under a rust

membrane at very low potentials. *Corros. Sci.* **36,** 479–483 (1994).

25. Sharland, S. M. & Tasker, P. W. A mathematical model of crevice and pitting corrosion-I. The physical model. *Corros. Sci.* **28,** 603–620 (1988).

26. Sharland, S. M. A mathematical model of the initiation of crevice corrosion in metals. *Corros. Sci.* **33,** 183–201 (1992).

27. Alavi, A. & Cottis, R. A. The determination of pH, potential and chloride concentration in corroding crevices on 304 stainless steel and 7475 aluminium alloy. *Corros. Sci.* **27,** 443–451 (1987).

28. Walton, J. C. Mathematical modeling of mass transport and chemical reaction in crevice and pitting corrosion. *Corros. Sci.* **30,** 915–928 (1990).

29. Walton, J. C., Cragnolino, G. & Kalandros, S. K. A numerical model of crevice corrosion for passive and active metals. *Corros. Sci.* **38,** 1–17 (1996).

30. Watson, M. & Postlethwaite, J. Numerical simulation of crevice corrosion of stainless steels and nickel alloys in chloride solutions. *Corrosion* **46,** 522–530 (1990).

31. Soltis, J. Passivity breakdown, pit initiation and propagation of pits in metallic materials – Review. *Corrosion Science* **90**, 5-22 (2015).

32. Stevens, N. Modelling chemical and geometric factors in corrosion. *Presentation* Slide-58 (2020).

33. Widodo, C. S., Sela, H., Santosa, D.R., The Effect of NaCl Concentration on the Ionic NaCl Solutions Electrical Impedance Value using Electrochemical Impedance Spectroscopy Methods. *AIP Conference Proceedings* (2018)

34. Matsushima, I., Sakai, J.I., Mechanism of crevice corrosion and its application in testing. *J.Iron Steel Inst. Jpn.* **63** (5), 598-604 (1977).

35. Mujanovic, E., Zajec, B., Legat, A., Kosec, T., Kovac, J., Mori, G., Honig, S., Zehethofer, G., Depassivation and repassivation of stainless steels by stepwise pH change. *Materials and Corrosion* **72**, 421-433 (2020).